Thermal Conductivity of Additively Manufactured Chopped Fiber Composite Materials

A thesis submitted by

Mohan John

in partial fulfillment of the requirements for the degree of

Master of Science

In

Mechanical Engineering

Tufts University

February 2026

Adviser: Dr. Anil Saigal

Thermal Conductivity of Additively Manufactured Chopped Fiber Composite Materials

Mohan John

Abstract

Thermal properties of additively manufactured composite materials are not as commonly studied as mechanical properties, dismissing processing considerations, and potential applications. Studies were performed to evaluate the thermal conductivity of chopped composite PA6-carbon fiber materials. Thermal conductivity was assessed for rectangular infill samples of increasing infill density. The effects of heat flow direction on thermal conductivity in the longitudinal and transverse directions in respect to the infill pattern geometry were also analyzed.

A steady state thermal conductivity technique based on ASTM standard D5470 was developed to evaluate the wholistic thermal impedance of non-isotropic materials. A positive relationship was discovered between infill density and thermal conductivity for transverse heat flow samples of infill between 10% to 77% and for longitudinal samples between 10% to 92%. The orientation of the chopped carbon fibers compared to the direction of system heat flow exhibited significant influence, with greater alignment facilitating higher effective thermal conductivity.

Adviser: Dr. Anil Saigal

Keywords

Additively Manufactured Composites, Chopped Fiber Composites, Thermal Conductivity, Steady-State Heat Transfer.

Nomenclature

Abbreviations:

CF	Carbon Fibers
CR	Contact Resistance
FDM	Fused Deposition Modeling
FEA	Finite Element Analysis
K	Thermal Conductivity
LCL	Lower Control Limit
MB	Meter Bar
PA6	Polyamide 6
Q	Heat Flow
ROM	Rule of Mixtures
TC	Thermocouple
UCL	Upper Control Limit

Acknowledgments

I would first like to thank Professor Anil Saigal for his impactful mentorship, insights, and guidance as well as Nikhilesh Rattan for his crucial efforts and meaningful contributions throughout this research endeavor. Thank you to Professor Ayse Asatekin and Professor Michael Zimmerman for their participation in the defense committee. A debt of gratitude is owed to Efe Inan for his groundwork research, knowledge, and equipment, and Dr. Marc Hodes for his thermodynamics insights that led to a successful test apparatus. Thank you to Dr. Michael Zimmerman for his composites and polymer science knowledge and for providing testing material, Hayden Colins for instruction regarding experimental equipment and data acquisition, and Samanta Carias and Vin Montuori for their support, use of the lab, and machine shop. Thank you to Addie Cotter for coordinating the acquisition of required materials. Additionally, thank you to my family for their encouragement and support throughout my graduate studies.

Mohan P. John

Tufts University

February 2026

Contents

List of Tables

List of Figures

Thermal Conductivity of Additively Manufactured Chopped Fiber Composite Materials

Chapter 1: Introduction

1.1 Motivation

Fused Deposition Modeling (FDM) printing is one of the most ubiquitous 3D printing methods. FDM printing involves thermoplastic-based filaments being heated, melted, and extruded through a nozzle onto a build plate layer by layer to create objects. FDM printing has existed since 1988 and through continued development has been adopted by professionals and made accessible to hobbyists. While FDM printing has geometric and prototyping capabilities that surpass subtractive manufacturing, product performance has always been limited by the materials they are printed from. Common printing thermoplastic polymers such as PLA, ABS, and TPU pale in comparison to the mechanical strength of metals, ceramics, and other thermoset polymers.

One method to improve the properties of FDM printed parts is through use of composite filaments that combine a thermoplastic matrix with the fibers of a stronger material, resulting in a combination of material properties. These reinforced composite filaments can produce FDM printed parts of comparable quality while having large improvements in mechanical properties.

A common composite FDM filament used to improve product mechanical performance is PA6-Carbon fiber filaments, combining chopped carbon fibers within a PA6 matrix [1]. While many studies have been performed investigating the composite mechanical properties, less work exists examining thermal properties and the effects of varying printing parameters. Quantifying thermal conductivity of this material opens opportunities for new applications and allows for better understanding of processing parameters that affect FDM chopped fiber composite thermal properties. For this study, the filament analyzed was the Markforged Onyx with a 20% volume

of chopped carbon fibers embedded within a PA6 thermoplastic matrix [2,3]. Test samples were printed using a Markforged Onyx Mark Two FDM printer.

1.2 Study Parameters and Research Scope

Infill is the internal structure of a 3D print. The infill material fills the walls and interior space between the exterior faces of the print. It provides structure and support and has considerable influence on a print's mechanical properties. The most common type of printing infill pattern is the rectangular, or grid, infill pattern. It is the default infill pattern for many slicer programs due to its balance of cost, strength, and print time.

Using the rectangular infill pattern, the relationships between infill density and thermal conductivity were evaluated by printing samples of increasing infill densities and finding their thermal conductivity.

Additionally, the effects of heat flow on thermal conductivity in the perpendicular and parallel directions to that of the infill patterns were also studied. For each infill density, samples with heat flow in the parallel and perpendicular directions were assessed to compare effects of infill orientation on effective thermal conductivity.

Using COMSOL Multiphysics, simulations were performed comparing the effects of infill densities and infill pattern orientations using a simplified hot meter bar setup to compare simulation trends to experimental data.

Finally, the thermal conductivity of FDM printed carbon fiber composite materials was compared to that of traditionally manufactured laminate carbon fiber to compare the effects of fiber geometries and production methods on thermal conductivity.

1.3 Literature Review

FDM manufacturing has grown in applications from rapid prototyping and proof of concepts to final product, engineering, and customer-facing applications. While many studies have been conducted to evaluate the properties and capabilities of FDM materials and products, most studies have focused on mechanical behaviors and the influence of processing techniques. In more recent years, there has been a rise in studies evaluating thermal properties of FDM printed materials, focusing on topics such as thermal diffusivity, conductivity, degradation, and influence of manufacturing defects. Recent examples from the past three years include work evaluating anisotropy, voids, and other processing effects on the thermal conductivity of polymer and fiber reinforced FDM materials [4]. Thermal conductivity studies also exist exploring the potential of electroplated FDM composite material thermal properties with various infill densities [5]. Earlier studies in Tufts University's mechanical engineering department involved evaluating the thermal effects of fiber reinforcement layers in FDM prints and linking their relationship to mechanical properties [6].

While studies on thermal properties of FDM composite materials have continued to grow, less work has been performed exploring chopped fiber composites and their relationships with infill density and the impact of heat flow direction. Additionally, while approaches such as the hot meter bar technique have risen as more common evaluation methods, there still does not exist a standardized framework for evaluating thermal conductivities of FDM printed samples.

Transient heat flow and steady state heat flow methods are the two main families of techniques used to evaluate thermal properties of materials. Transient heat flow methods involve short pulses of concentrated heat that disperse throughout the sample. The thermal response over

time is used to find thermal properties of the sample. Transient testing is significantly faster than steady state methods and usually has less heat loss to the environment.

Steady state heat flow methods require a constant heat flow and temperature gradient through a sample. Thermal properties are found from the sample's surface temperatures, heat flow rate, and thickness. This method can provide better analysis of bulk conductivities for non-isotropic samples [7]. FDM manufactured materials are at most orthotropic and have consistent properties in three different plane directions and not throughout the entire material due to the filament layup process. Additionally, samples will need to be relatively thick compared to average thermal testing specimens to capture the effects of infill density and influence of air pockets. Steady state methods can measure conductivity between 0.1 and 100 W/mK and encompasses the expected range of the composite filament [8]. With these considerations, a steady state heat transfer method was implemented for this study.

To create a steady state heat transfer setup, ASTM D5470 "Standard Test Method for Thermal Transmission Properties of Thermally Conductive Electrical Insulation Materials" was adapted for use with printed FDM samples. Using work documented in literature, ASTM D5470, and hardware from Inan's previous setup, a guarded hot plate steady state heat transfer apparatus was developed. This apparatus involved the use of a heat source and heat sink connected to two high conductivity reference material meter bars on either side of the test sample. Using thermocouples imbedded within the reference meter bars, the sample surface temperature and heat flow rate are determined and used to calculate sample thermal impedance.

A reference material with a thermal conductivity of at least 50 W/mK is recommended [9]. Copper is a common choice while other setups use aluminum as an alternative. For this

study, a copper meter bar will provide better data accuracy for samples within the expected material conductivity ranges [10].

An important consideration is the effects of thermal contact resistance at the interfaces between the sample and meter bars. Contact resistance is caused by surface roughness of the connecting surfaces, creating imperfect contact between the interfaces. This results in less conduction between the two surfaces and small air gaps that cause convective heat transfer between the mediums, resulting in reduced heat transfer and increased resistance. To mitigate these effects in thermal conductivity calculations, two samples of different thicknesses are needed for each data point. Computing the reciprocal of the rate of change of thermal impedance between different sample heights removes these effects from results [9].

Since the effects of contact resistance will be removed using multiple samples per data point, it is imperative that contact resistance between samples is consistent. Differences in applied loads cause great differences in resulting conductivities [11]. Another crucial element is to ensure proper alignment of samples, as even slight misalignment between the faces of the meter bar and test samples can result in mistrials. Taking these principles into account, an experimental apparatus and test plan was developed for this study.

Chapter 2: Infill Pattern, Heat-flow Orientation, and Thermal Conductivity Framework

2.1 Infill Pattern, Densities, and Sample Sizes

Samples of rectangular infill patterns of increasing infill densities were printed and evaluated. Rectangular infill geometry consists of sets of perpendicular layers of infill that create a grid structure. Compared to other geometries, rectangular infill offers a balance of fast print speed and reduced material consumption while providing reasonable mechanical strength. Due to its ubiquitous use, it was the chosen infill pattern for this study.

Samples with infill patterns of 10, 33, 55, 77, 92, and 100% infill were assessed. Geometries and infill densities are summarized in Fig 1.

Infill Density	10%	33%	55%	77%	92%	100%
Infill Geometry View (1 X 1 cm)						
Sample View (4.57 X 4.57 cm)						

Fig. 1. Infill densities of test samples.

Most steady state thermal conductivity testing setups involve samples that are around 1 mm or less thick. Samples with heights of 1 mm or less will not be able to quantify the effects infill pattern on thermal conductivity as the thickness of the infill region will be negligible in size compared to the sample roof and floor surfaces. Using the standard slicer recommended floor

and roof thicknesses, a 1 mm height sample will only have the infill region account for 20% of the sample volume. This will result in conductivity differences that are difficult to quantify due to lack of thermal behavior being influenced by the infill region and pattern. However, too tall of a sample will result in heat loss to the environment and impact data accuracy.

Sample heights of 5 mm and 10 mm were chosen to balance having a sample height large enough for effective thermal properties to be influenced by the infill region while still being relatively short to minimize environmental heat loss. Two sample heights per data point were required to mitigate contact resistance in thermal conductivity calculations. The sample faces were 1.8 in x 1.8 in (45.72 mm x 45.72 mm) squares. Fig 2 depicts test sample geometries and dimensions.

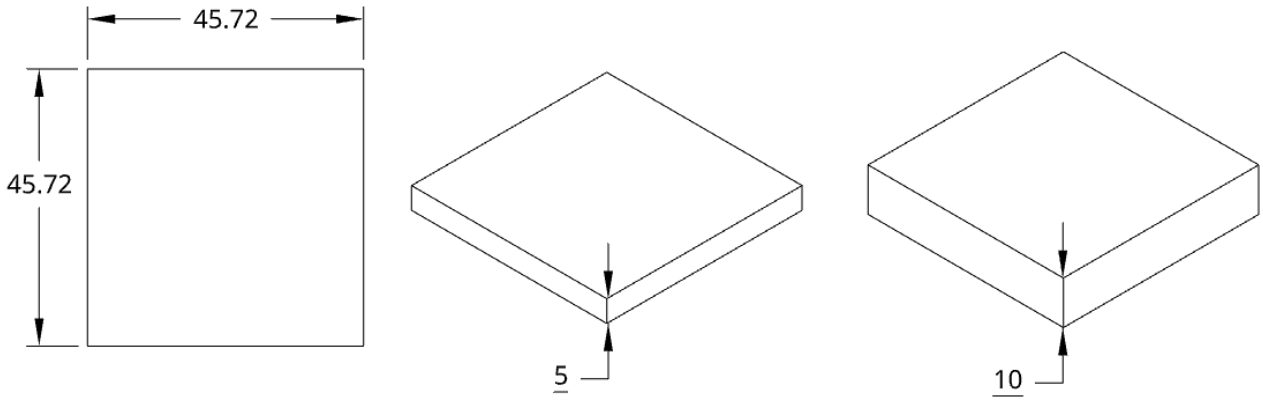

Fig. 2. Diagram of test samples. Dimensions in mm.

2.2 Infill Orientations and Direction of Heat Flow

The thermal conductivity with system heat flow in the transverse and longitudinal directions of the infill pattern were studied. The longitudinal direction is defined as along the direction of the plane of the rectangular grid. The transverse direction is defined as perpendicular to the infill pattern plane and into the rectangular grid. Fig 3 illustrates these two directions.

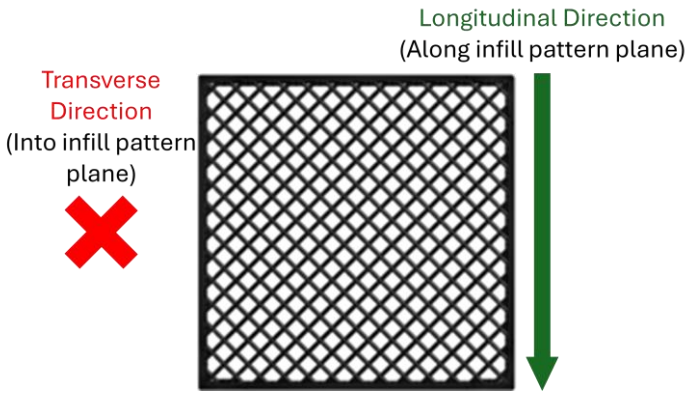

Fig. 3. Longitudinal direction (green) in the direction of the infill layup and transverse direction (red) in the perpendicular direction of the infill plane.

Sample for each infill density were tested with heat flow along both longitudinal and transverse directions. With respect to the experimental setup, heat flow in the longitudinal direction travels downwards from the hot to cold sample faces along the infill channels at a positive and negative 45-degree angle. The direction of heat flow is perpendicular to the direction in which the sample is built. In the case of transverse samples, the heat flows downwards into the infill pattern grid through channels that extend from the hot to cold surface that are parallel to the sample walls and heat flow direction. The direction of heat flow is in line with the direction that the sample is built. These directions of heat transfer are depicted in Fig 4.

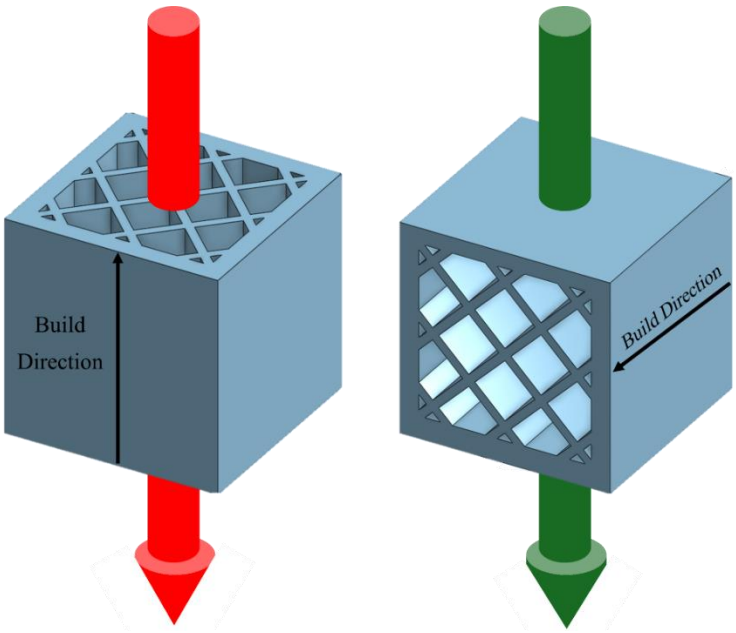

Fig. 4. Isometric view of longitudinal system heat flow (green) in the direction of the infill plane and transverse system heat flow (red) in the perpendicular direction.

2.3 Sample Printing and Processing Conditions

A Markforged Onyx Mark Two FDM printer was used to produce test samples. Experimental data was evaluated from samples processed under the following conditions described.

Samples were printed from the Onyx PA6-CF composite filament extruded from the 0.4 mm nozzle head with extrusion temperatures of 280 ºC onto an unheated bed within an enclosed chamber. Within the Markforged Eiger slicer, samples were set to print with roof and floor layers set to 4 for a thickness of 0.4 mm. The wall thickness was set to 2 for a thickness of 0.80 mm. Layer thickness was set to 0.100 mm. Printing speeds were the default settings for Onyx filament determined by the slicer. The rectangular fill pattern was used for slicing the 10, 33, 55, 77, and 92% infill samples. For the 100% infill density the solid fill option was selected. For each tested

infill density, a longitudinal and transverse sample was printed. For each orientation and infill density combination, a short (5 mm) and tall (10 mm) sample were printed. In total 24 samples were created and evaluated. No postprocessing for Onyx printed parts was necessary.

Filament was stored in a dry box lined with desiccant packs to prevent moisture contamination. Before each sample print, a purge of filament left in the system from the prior print was performed to ensure no printing was performed with moisture contaminated material. The printer and dry box setup can be seen in Fig 5.

Fig. 5. The Markforged Onyx Mark Two printer and dry boxes to store filament.

To print a transverse specimen, the sample was printed with its large faces parallel to the print bed. This print orientation results in an infill pattern that will be in the transverse heat flow direction during testing. The transverse sample build process is shown in Fig 6.

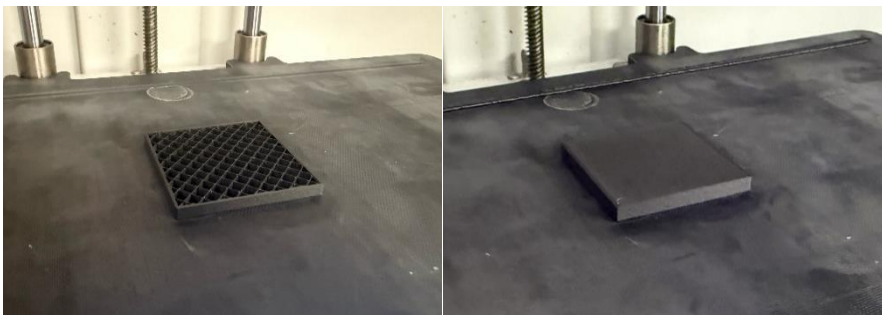

Fig. 6. Sample printed in the transverse infill orientation mid print and after completion.

To create longitudinal infill patterns, the samples were rotated 90 degrees when printed to have their short faces on the bed plane. This orientation results in the infill pattern being longitudinal to the heat flow direction when the samples are rotated back to their flat orientations for testing. Longitudinal printing orientation can be seen in Fig 7.

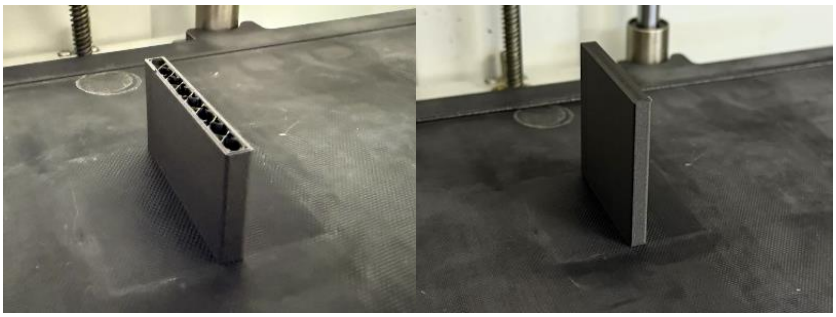

Fig. 7. Sample printed in the longitudinal infill orientation mid print and after completion.

2.4 Steady-State Heat Transfer Method to Determine Thermal Properties

ASTM standard D5470 outlines a measurement method using a guarded hot plate technique and meter bars to find the thermal impedance of thermal interface materials. The standard was adapted to find the thermal conductivity of printed composite samples by creating a similar experimental setup and employing the same thermal impedance evaluation and calculation methods.

To analyze sample conductivity the technique requires creating consistent steady state heat flow through a sample between meter bars that are of a known thermal conductivity. Using these reference thermal conductivity meter bars, the heat flow through the sample and the sample surface temperatures are evaluated and used to calculate sample thermal impedance and conductivity. Fig 8 depicts a simplified guarded hot plate setup.

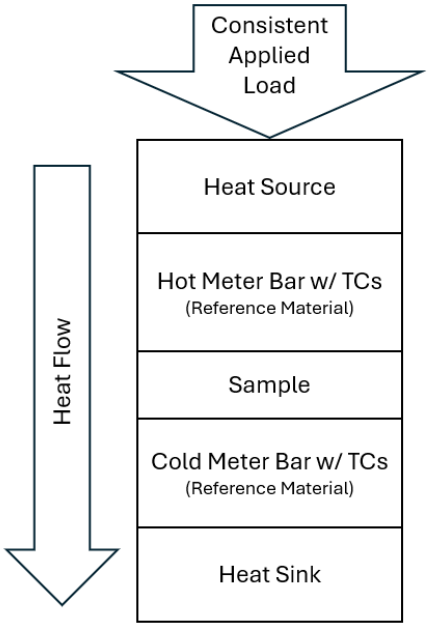

Fig. 8. Simplified depiction of steady state guarded hot plate testing setup.

To calculate thermal conductivity, what first is needed is the rate of temperature change through the height of the hot and cold meter bars. The rate of temperature change within each meter bar (*dT/dH*) is calculated by performing a linear regression fit of the thermocouple temperature readings over the distance they are spaced within the meter bars and obtaining the slope. From dT/dH, the heat flow ($Q_{hot,}$ Q_{cold}) for each meter bar is calculated using the meter bar and sample contact surface area (A) and the meter bar thermal conductivity ($Ref\ k$).

$$Q_{hot}\ , Q_{cold}(W) = \frac{dT}{dH} * A * Ref\ k \tag{2.4.1}$$

From the hot and cold meter bar heat flow, the average sample heat flow (Q) is taken as the average of both heat flow rates.

$$Q(W) = \frac{Q_{hot} + Q_{cold}}{2} \tag{2.4.2}$$

The sample surface temperatures are equivalent to the intercept of the regression fit for the hot and cold meter bars. Using the sample hot surface temperature (*Temp. H*), cold surface

temperature (*Temp. C*), sample height (h), and the heat flow rate (Q), the thermal impedance (θ) is calculated.

$$\theta\left(\frac{K*m^2}{W}\right) = \frac{A}{Q} * (Temp.H - Temp.C) \tag{2.4.3}$$

Due to surface roughness of the sample and the meter bars, contact resistance exists between their interfaces and results in an increase in thermal resistance. Surface roughness causes inconsistent contact between the surfaces and therefore results in less conduction while increasing convective air pockets at the interface. To mitigate these effects, two samples of different heights were tested for each data point. True thermal conductivity (k_{sample}) is calculated by calculating the rate of change between impedance and sample heights (h) and taking the reciprocal.

$$k_{sample}\left(\frac{W}{mK}\right) = \frac{1}{\frac{\theta_{tall} - \theta_{short}}{h_{tall} - h_{short}}} \tag{2.4.4}$$

Chapter 3: Experimental Setup, Procedures, Testing

3.1 Overview of Experimental Setup Improvements

In an earlier study, a steady state guarded hot plate test apparatus was created to prove theoretical relationships linking mechanical and thermal properties of continuous carbon fiber composite printed materials by Inan [6]. However, the system did not have the precision or resolution to detect the more subtle differences in thermal conductivity between varying infill density samples. Using other steady state experimental setups as reference and input from Inan and Hodes, the setup was improved upon to increase capabilities. These changes are summarized in Table 1. Fig. 9 shows the original and improved experimental setups.

Table 1. Summary of improvements made to the existing experimental setup.

System Attribute	Original System	Improved System
Clamping Method	4 wing nuts on threaded rods compressing central spring	Overhead central screw clamp
Load Measurement	4 load cells at each wing nut arm measuring deflection	Digital scale beneath applied load measuring clamping force
Meter Bar Material	HDPE (0.396 W/mK)	110 Copper (390.89 W/mK)
Meter Bar Lengths	90 mm and 20 mm	120 mm and 50 mm
Thermocouples	3 hot and 2 cold	3 hot and 3 cold
Paste Deposition	By hand w/ spatula	Stencil deposition method
Insulation Method	Polystyrene thermal jacket for meter bar stack	Double wrapped fiberglass insulation for meter bar stack and entire system
Sample Heights	45 mm and 65 mm	5 mm and 10 mm

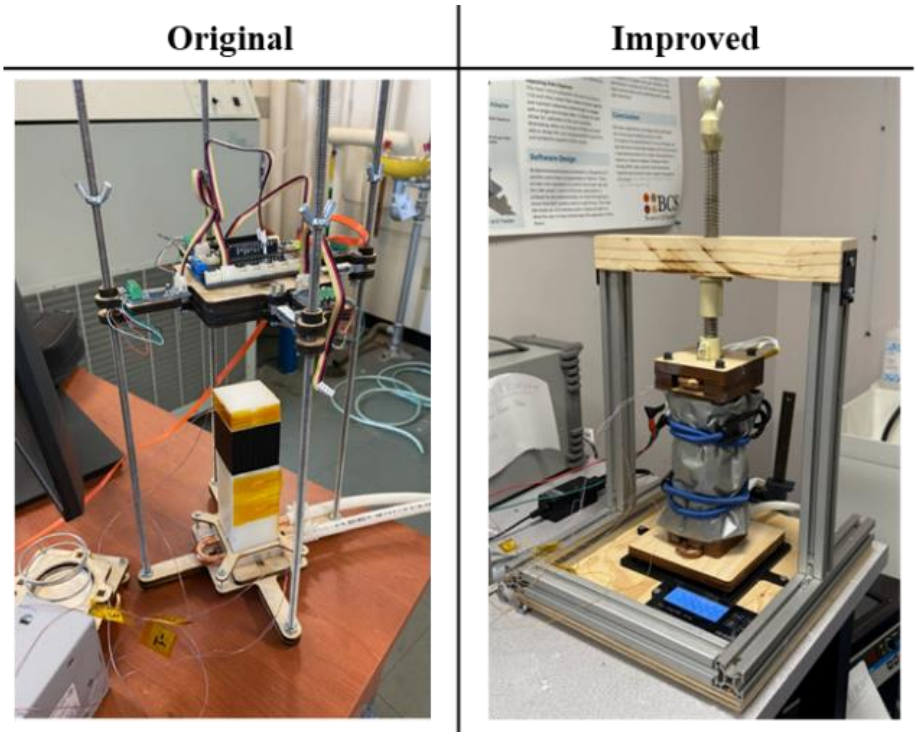

Fig. 9. Original and improved experimental setups.

3.2 Meter Bar Material and Construction

A new meter bar material with higher thermal conductivity was selected. The final material chosen was 110 Copper with a thermal conductivity of 390.89 W/mK [12]. Copper has high thermal conductivity, is relatively easy to source compared to other high conductivity metals and exceeds the ASTM D5470 recommended minimum conductivity of 50 W/mK. Copper was chosen over aluminum as a reference material to reduce measurement error [10]. Initially in the study, 303 stainless steel was chosen as the new meter bar material with a thermal conductivity of 16.2 W/mK. This material was first chosen under the assumption that a reference material closer to the thermal conductivity of the expected sample would provide more accurate data. While the data collected with the steel meter bar showed a significant improvement in

accuracy over the original HDPE bar's results due to having a higher thermal conductivity, the data was not precise enough to conclusively differentiate sample conductivities.

Using a milling machine the width and depth of the meter bars were machined to a length of 1.8 +/-0.005 in. To help mitigate the effects of inconsistent contact resistance the top and bottom faces of both meter bars were machined using a face mill for a smooth surface finish. The length of the meter bar significantly influences the linearity of its rate of change of temperature [13]. Using COMSOL Multiphysics simulations, it was concluded that after approximately a distance of 100 mm from a heat source the change in temperature within the meter bar decayed at a much more linear rate than after the interface between the hot meter bar and heat source. To align with the hot meter bar length chosen by Kempers et al for their high precision setup, a final hot meter bar length of 120 mm was selected. With this length the rate of change in temperature in the meter bar (*dT/dH*) would be more linear, allowing the linear regression approximation for the change in temperature to be a more accurate fit. Correctly gauging the dT/dH for the meter bars is critical to find heat flow and the sample surface temperatures, improving thermal conductivity calculations. In a previous meter bar iteration, a hot meter bar length of 50 mm was used. With such a short meter bar the dT/dH linear approximation could not accurately model the curve of temperature change through the meter bar. This resulted in inaccurate surface temperature and heat flow values that provided poor conductivity data.

K and T type thermocouples were used to determine meter bar temperatures and were connected to a National Instruments cDAQ-9174. The hot meter bar was connected to an aluminum hot plate heated by two cartridge resistor heaters. Three thermocouples were placed in the hot meter bar at positions of 5, 25 and 45 mm away from the sample surface. Thermocouple holes were drilled using a #49 drill bit to a depth of 0.6 in (15.24 mm). A plate with three plugs

was printed from PLA to secure the thermocouples in place, as seen in Fig 10. With the plate in place, tension on the thermocouple wires was concentrated to the contact point with the plate at the entrance of the holes and prevented the thermocouple tips within the meter bar from being displaced.

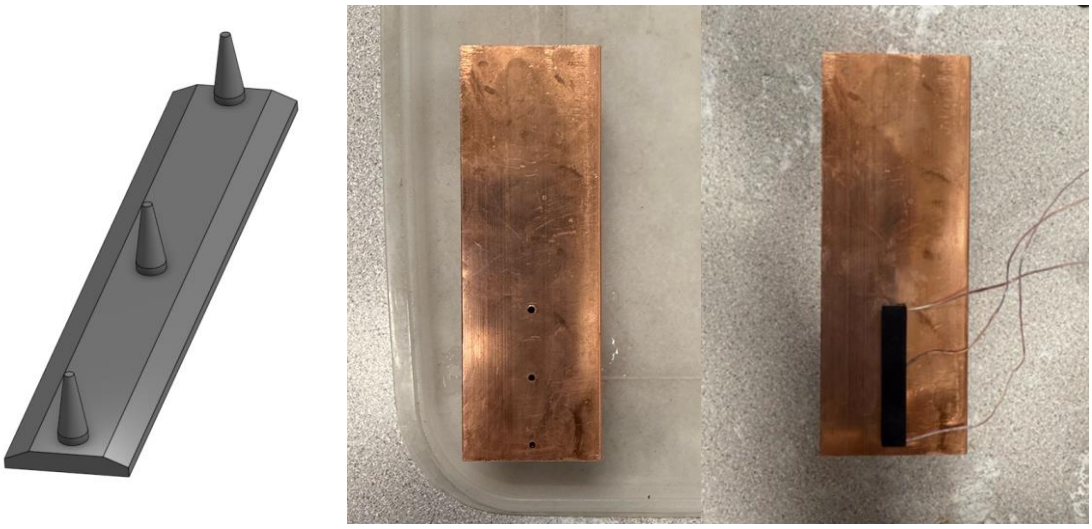

Fig. 10. Plug to secure thermocouples (L), Hot copper meter bar with thermocouple holes (M), Hot meter bar with thermocouples secured by plug (R).

From the LabVIEW data output, it was observed that the thermocouple readings oscillate by a maximum of +/-0.06 °C. Due to copper's high thermal conductivity there is a much smaller change in temperature throughout the meter bar. If thermocouples are not spaced a sufficient distance the data will have significant error when determining dT/dH due to temperatures not having a substantial difference, allowing their values to be heavily influenced by noise. Spreading apart the thermocouple positions will provide readings with greater differences in temperatures and therefore will be less influenced by noise in the data. However, the further spaced the thermocouples are the less accurate dT/dH will be to the true change in temperature going into the sample surface, affecting heat flow and surface temperature approximations. Using COMSOL simulation data it was determined that a 20 mm spacing between each

thermocouple provided the most optimal balance of a having a large enough difference in temperature readings to not be drastically affected by noise (a maximum of 26% compared to average difference in temperatures) while still being fairly close together to provide a reasonable estimate of dT/dH. Fig 11 compares results of simulated thermocouple spacing. Thermal conductivity values and dT/dH at different thermocouple spacings were calculated by using temperature values from the simulation at the positions of the thermocouples with the calculation methods discussed in section 2.4. The influence from the thermocouple noise was quantified by the proportion of maximum observed noise (0.06 °C) to that of the average temperature difference between simulated thermocouple readings.

$$Data\ Impact\ From\ Noise\ (\%) = \frac{Maximum\ Observed\ Noise}{\frac{[(TC1-TC2)+(TC2-TC3)]}{2}} * 100 \qquad (3.2.1)$$

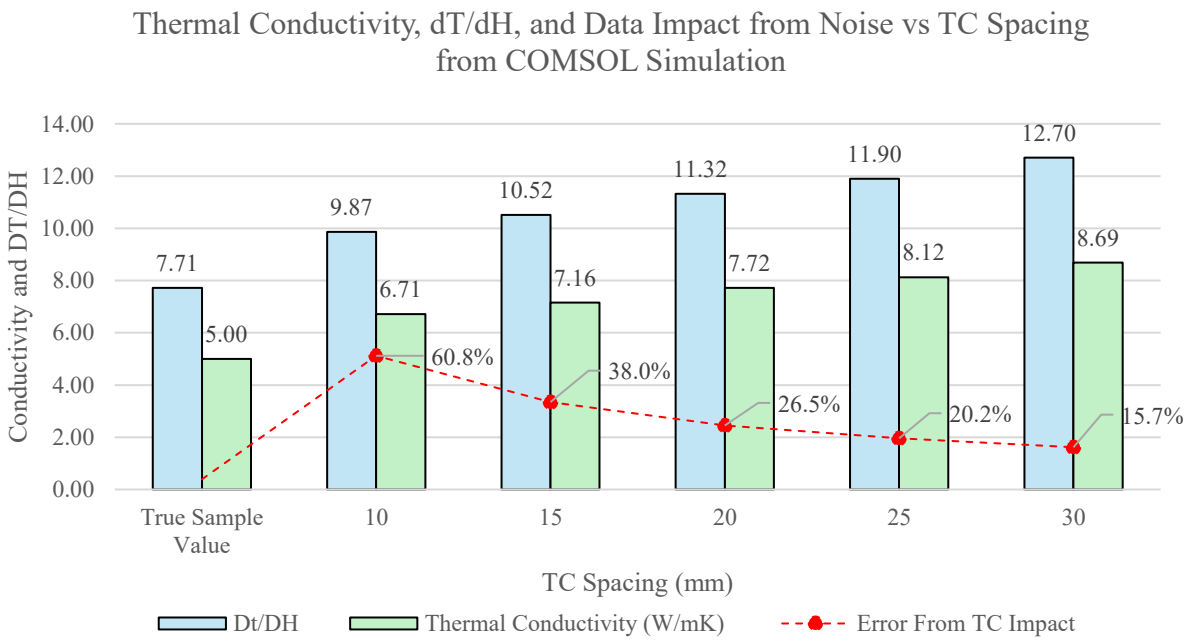

Fig. 11. Simulation comparison of accuracy and noise tradeoffs of TC spacing.

It is crucial for accuracy of the system to have a hot meter bar long enough in length to allow for a more linear reduction in temperature by end of the meter bar flowing into the sample.

For the cold meter bar, it is less essential to have a large length since thermocouple placements are near where heat leaves from the cold sample side to gauge the heat flow out of the sample. Therefore, a large length to reach linearity is not needed since temperature readings must be taken as close to the sample surface as possible. Minor differences were noted in COMSOL simulations between cold meter bar simulations of varying sizes (120 mm, 100 mm, 50 mm). A length of 50 mm was chosen to conserve material. A third thermocouple was added to the cold meter bar to provide more accurate estimations of dT/dH and surface temperature approximations. Thermocouples were spaced 5, 20, and 35 mm from the cold sample surface. The cold meter bar is seen in Fig 12.

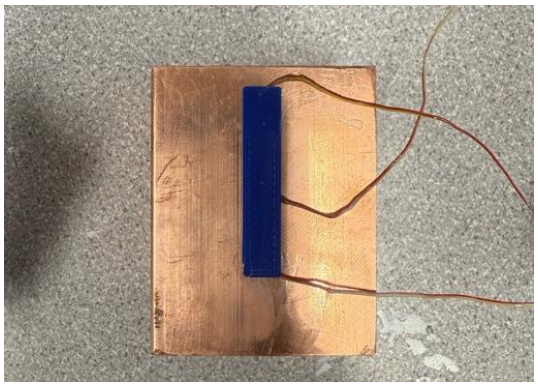

Fig. 12. Cold meter bar with plug to secure thermocouples.

3.3 Providing Consistent Load and Contact Resistance

A screw clamp was used to provide a constant applied load on the meter bar stack and sample in a similar method to other steady state setups [14]. The screw clamp was secured to the apparatus frame constructed of 8020 aluminum beams mounted to a 1” (2.54 cm) thick plywood base. A digital scale was slotted into an acrylic bracket on the top of the base plate to measure applied load. On top of the scale, the meter bar and sample stack were mounted using a bracket that was fixed to the scale. An alignment guide from laser cut birch wood was implemented into

the top of the cold plate bracket to prevent misalignment between the samples and meter bars while also providing added insulation. This system provided more consistent and higher load than the previous clamping system, which provided force from four sides of the sample with threaded rods and wing nuts onto a spring. Additionally, implementing a digital scale in line and centered with the applied force improves accuracy in measuring clamping load rather than using the four load cells to measure deflection at each clamping screw. Thermal grease was used at every heat transferring interface to reduce contact resistance and promote optimal heat flow. Fig 13 shows the test apparatus and configuration of the meter bar stack.

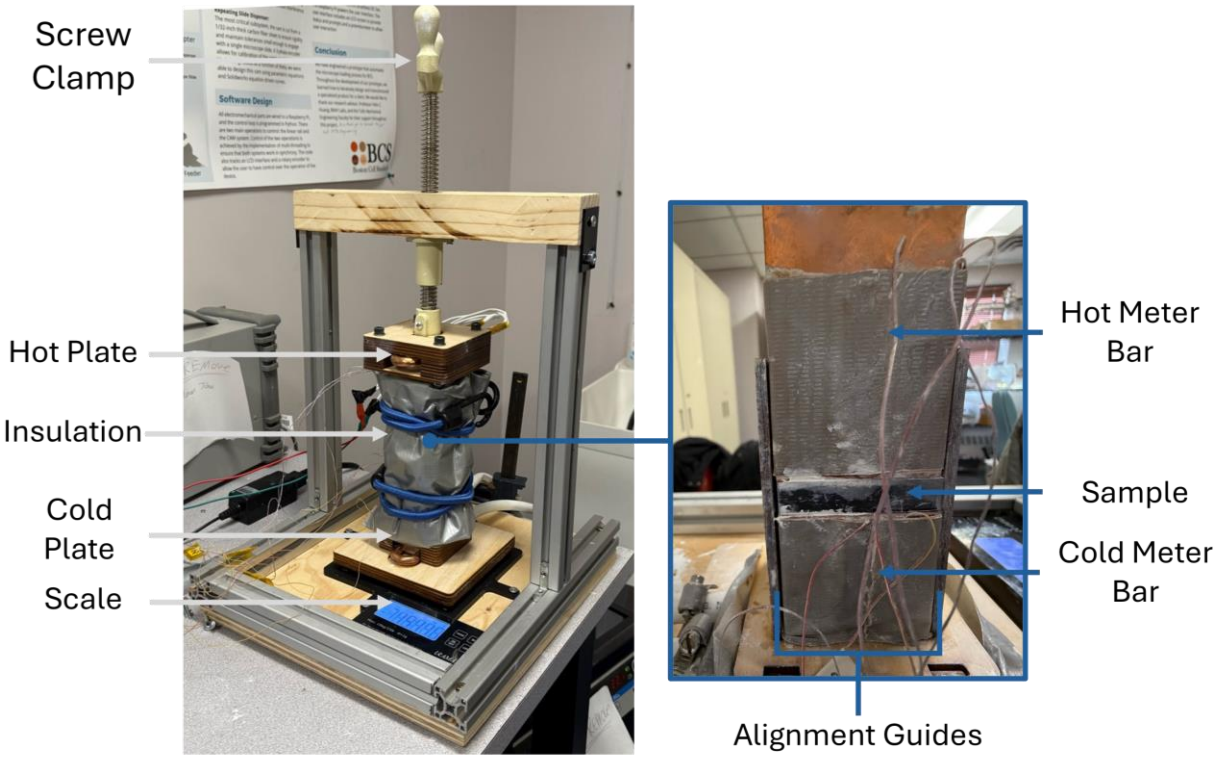

Fig. 13. Test Apparatus and Meter Bar Stack diagram.

For thermal conductivity calculations it is crucial to ensure that both samples in a set have consistent contact resistance. The major factors that influence contact resistance in a steady state setup are the applied clamping load and the thermal interface medium.

Halnziye HY400 thermal grease was applied to both ends of the sample in contact with the meter bar. A stencil was used to ensure a consistent amount of thermal grease was applied between samples, as seen in Fig 14. The stencil was printed from PLA and had apertures with the volume of the desired deposited volume of thermal grease. A guide was also printed to suspend the sample by the edges to apply paste to both sides without contact with the table surface.

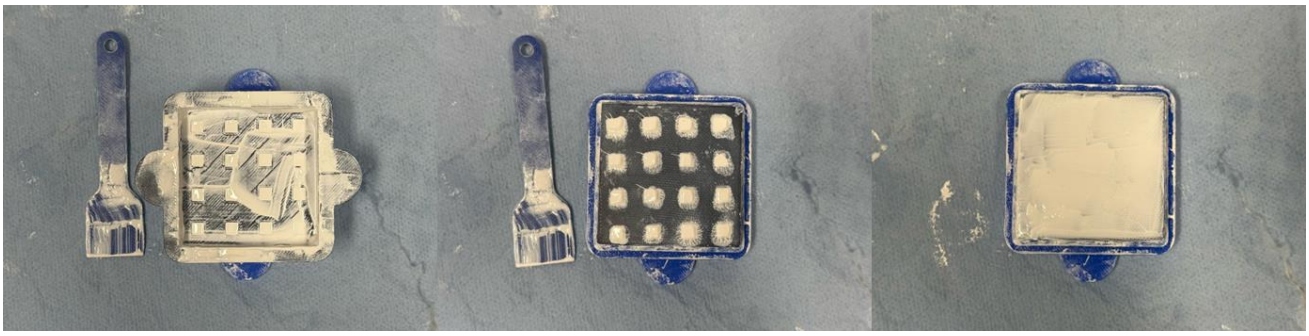

Fig. 14. Stencil grease deposition process. Stencil is placed onto sample, grease is spread through apertures and removed, grease is spread evenly onto sample surface.

Each sample had an applied clamping load of 15 kg (147.15 Newtons). Using the digital scale clamping force was able to be measured up to 1 gram (0.00981 N) in accuracy. Using consistent paste and applied force between samples increased accuracy of thermal conductivity calculations due to consistent contact resistance.

3.4 System and Sample Insulation

Proper system insulation is critical to prevent heat loss to the environment and to achieve one-dimensional steady state heat flow through the system. To provide the necessary environmental isolation, insulation sleeves were constructed. Fiberglass insulation rolls ¾ inch thick were cut into sections the length necessary to encompass the entire system. The fiberglass was wrapped with a layer of plastic peel ply fabric to contain the fibers. The exterior was

covered in a duct-tape shell to hold the fabric and fiberglass together and provide added insulation. The insulation sleeve and components can be seen in Fig 15.

Fig. 15. Fiber glass sheet (Top). Insulation wrapped in duct tape and fabric sleeve (Bottom).

Two sleeves were created to wrap the system. One sleeve encompassed the meter bar and sample stack while the second was wrapped around the first layer and the entire system and heater block. This setup is shown in Fig 16. Additionally, the tested sample sizes were reduced from the previously used 67.5 mm and 45 mm sample heights to 10 mm and 5 mm to reduce environmental heat loss and improve measurement capabilities. During testing when the hot meter bar registered temperatures around 60 ℃, the exterior of the inner and outer layers was measured using a FLUKE digital thermometer. The outer surface of the first insulation sleeve layer exhibited temperatures between 26 and 27 ℃ while the outer surface of the second layer was between 24 and 25℃. The environmental temperature during testing was between 23 and 24 ℃. The marginal difference between environmental temperatures and the insulation sleeves shows their effectiveness.

3.5 Overall Experimental Setup and Equipment

The following figures depict the overall experimental setup and necessary hardware. A schematic of the overall system illustrating how systems interact is shown in Fig 16. In Fig 17 and 18 the power supply, chiller, and DAQ used for testing are shown.

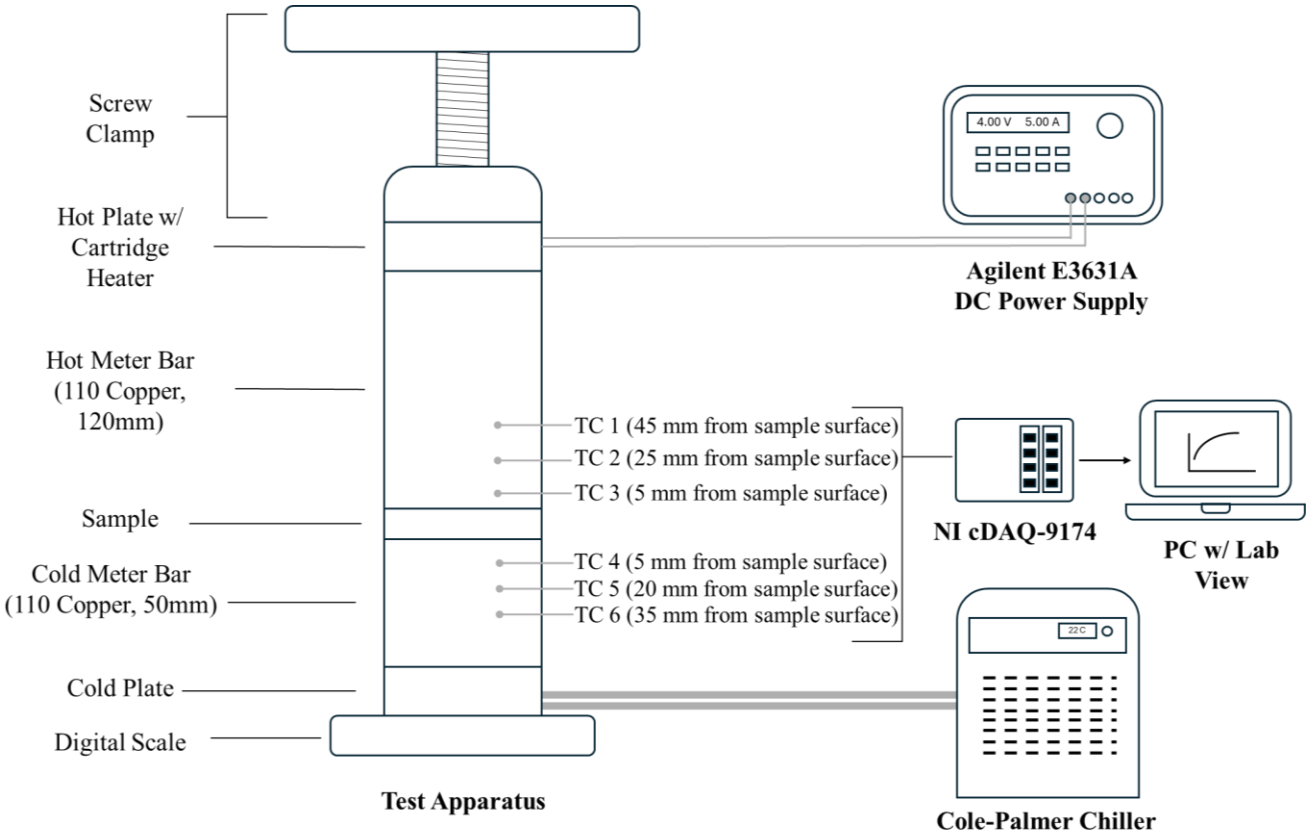

Fig. 16. Experimental setup diagram with test apparatus, data acquisition unit, heater, and chiller.

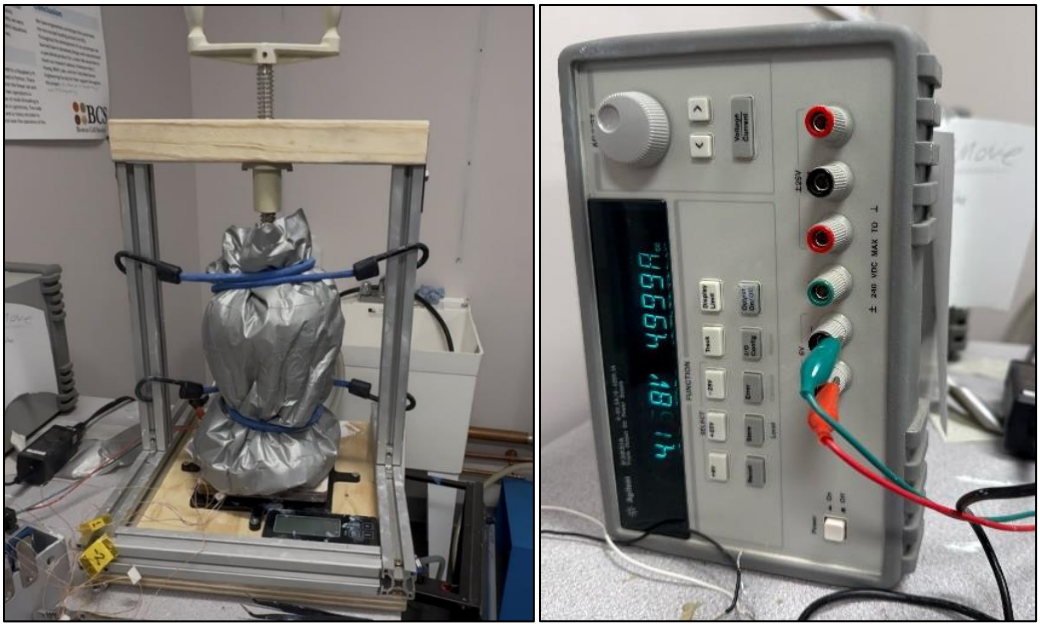

Fig. 17. Insulated steady-state test apparatus during testing (L) and Agilent E3631A Power supply connected to cartridge resistance heater (R).

Fig. 18. National Instruments DAQ system (L) and Cole Palmer recirculating chiller (R).

3.6 Experimental Procedures

The following outlines the experimental procedure conducted during this study:

1. Sample Preparation
    a. Place sample onto the holding fixture.
    b. Place stencil on top of the sample. Apply thermal grease to stencil and spread paste evenly into each aperture using the spatula.
    c. Remove the stencil from sample face. Rotate the sample to show the opposite face and place the sample back onto the holding fixture.
    d. Place stencil on top of the second face. Apply thermal grease using the spatula.
    e. Remove the stencil from the face of the sample. Spread grease evenly on both sides of the sample to cover the entire face with a thin layer of paste.
2. Loading Sample and Applying Clamping Load
    a. Clean off any residual grease left from previous trials from the interface between the meter bars and sample.
    b. Place the sample onto the face of the cold meter bar and push the sample inwards until it aligns with the alignment guide.
    c. Turn on the digital scale. Set the current weight to zero.
    d. Turn the handle of the screw clamp clockwise until the face of the hot meter bar reaches the sample surface.
    e. Slowly increase the load and compress the sample until the digital readout reaches an applied load of 15 kg.
3. Applying Insulation Wrap
    a. Take the inner insulation sleeve and wrap it around the meter bar and sample stack.

b. Secure the sleeve with a Velcro strap at the top around the hot meter bar and at the bottom around the cold meter bar.
c. Wrap the inner insulation sleeve with the larger outer insulation sleeve, encompassing the heater and cold plate.
d. Secure the sleeve using bungee cords at the point above the hot plate bracket and below around the base plate of the cold meter bar. Attach the cord tips to the crevices in the aluminum posts holding the screw clamp.

4. Starting the Experiment
    a. Turn on the power supply unit. Set the output current to the maximum (4V, 5 Amps).
    b. Add water to the chiller reservoir if needed. Start the chiller. Set the temperature to the ambient temperature.
    c. Connect the DAQ USB to a computer. Launch the appropriate LabView program. Assign data inputs for TCs to their correct DAQ channel.
5. Acquiring Data
    a. Run the experiment until steady state heat flow has been achieved.
    b. Export the data to a spreadsheet program.
    c. Determine the final temperature values for calculations for each thermocouple by taking an average over ten minutes of steady state.

To ensure steady state heat transfer had been reached, the experiments were allowed to run for at least 6 hours and up to 24 hours. ASTM standard D5470 states that steady state is reached no change greater than 0.1 ℃ in recorded temperature over a course of five minutes. For this study, the time was doubled to ten minutes to ensure accuracy. Additionally, the data points

for evaluation were taken as an average thermocouple value over the course of the steady state period to help mitigate the effects of noise from thermocouple readings.

3.7 Evaluating System Accuracy and Stencil/Thermal Grease Effectiveness for Consistent Contact Resistance

To evaluate the accuracy of experimental thermal conductivity values obtained, a trial was conducted using 303 steel with a known thermal conductivity of 16.2 W/mK [15]. Two samples approximately 5 mm and 10 mm in height with the same area as the test samples were produced and assessed. The results are summarized in table 2.

Table 2. Experimental and expected thermal conductivities of 303 steel and acrylic.

Parameter	Value
Expected K (W/mK)	16.2
Experimental K (W/mK)	20.72
Percent Error	27.88%

The experimental value for the 303-steel sample had an error of 27.88% with a thermal conductivity value 4.52 W/mK greater than the expected value. From this difference the estimated system overshoot is approximately 27.88%. This difference can be used as a proposed correction factor to obtain true thermal conductivity values.

$$Corrected\ K = \frac{K\ Experimental}{1.2788} \tag{3.7.1}$$

For consistency, the data of this study will be presented as the raw system thermal conductivity without the correction factor adjustment. The correction factor will require more trials of materials with known conductivities to fully quantify the system error. While the obtained experimental values may not represent the absolute thermal conductivity of the tested

samples, the system has the consistency and resolution to provide relative comparisons between samples and analysis of trends.

An extruded isotropic acrylic sample was tested to gauge the ability of the system to quantify low thermal conductivity samples and the effectiveness of the stencil and thermal grease setup at providing consistent contact resistance and data improvements. To confirm that the thermal grease was contributing to maintaining consistent contact resistance, samples without thermal grease were trialed. Both samples were laser cut from extruded sheets of 1.5 mm and 3 mm in thickness and did not have their depths machined. This ensured that both sample faces in contact with the meter bar had a smooth finish untouched by further machining with as low as a surface roughness as possible. For the first set of trials neither sample had thermal grease applied. For the second set of trials the stencil method was used for grease deposition on both samples. Table 3 and Fig 19 summarize the results.

Table 3. Acrylic trials with and without thermal grease.

Acrylic Sample Trial	**Thermal Conductivity (W/mK)**	**Thermal Interfacial Resistance – Ri ($K*m^2/W$)**
Without Thermal Grease	1.75	0.0030
With Grease	1.01	0.0020
Expected Value	0.200	-

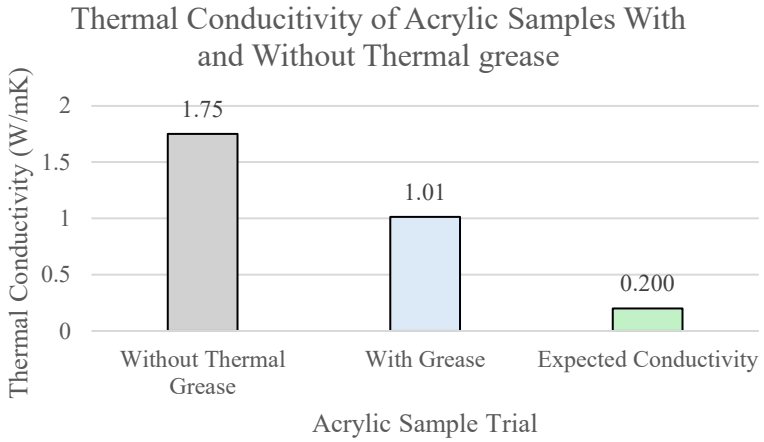

Fig. 19. Comparison of acrylic thermal conductivities with and without thermal grease.

The conductivity of the trial without thermal grease was less accurate compared to the true thermal conductivity of the acrylic and 72.7% greater than the trial containing thermal grease. This reduction in accuracy is attributed to inconsistent contact resistance between the thin and thick samples, as this will skew the calculated thermal conductivity when contact resistance is offset in calculations. Additionally, the thermal interfacial resistance of the trial without thermal grease was greater than that of the trial with grease. Therefore, even with a smooth surface finish the interfacial resistance of the sample was reduced by use of the thermal grease.

The acrylic sample with the standard grease application method presented the lowest thermal conductivity out of all test samples in the study. However, the recorded value of 1.01 was still greater than the expected thermal conductivity of 0.200 W/mK [16]. Therefore, the system likely has a lower measurable conductivity threshold of approximately 1.01W/mK.

3.8 Experimental Setup Successes and Limitations

Compared to the original system, the new system had the resolution, precision, and accuracy needed to quantify the more minute differences seen in thermal conductivity between

samples of different infill density and orientation. The new screw clamping method provided an efficient method to load and unload samples from the test apparatus and reduced setup time. The use of a digital scale measuring a force directly underneath the applied load improved load measurement and accuracy. A digital force readout provided a more convenient method to monitor sample load than manually checking four load cells using an Arduino python program and adjusting the individual clamping points. The stencil deposition method of paste reduced variability in contact resistance between tall and short samples, improving calculation accuracy.

While the new system provides significant improvements over the original setup, the system still has notable limitations. Evaluated thermal conductivities are likely overestimates by 27.88% and the lower limit of recordable thermal conductivities is approximately 1.0 W/mK. This overshoot in thermal conductivity and inability to quantify very low thermal conductivities is likely attributed to the thermocouple spacing within the meter bars. As discussed previously in section 3.2 and shown in Fig 11, the thermocouples were spaced a distance of 20 mm apart to help mitigate the effects of noise in temperature readings. Data noise at thermocouple points spaced in close proximity can ruin dT/dH approximations and surface temperature values due to the noise having a larger influence skewing data since the temperature differences between the thermocouples will be minor. While the chosen spacing reduces the impact of noise, it also results in lower surface temperature approximations. This reduces the difference in hot and cold face sample temperatures (*Temp.H and Temp.C*), increasing the calculated thermal conductivity. The further spacing of the thermocouples results in the linear approximation of temperature change being taken from points before the most linear region in the meter bar. Therefore, the linear approximation slope is steeper than the true change in meter bar temperature going into the sample. This results in a greater dT/dH and crucially a lower estimated surface temperature. As

depicted in Fig 11 from the COMSOL simulated results, increasing the distance between thermocouples increases the estimated thermal conductivity compared to the true conductivity. Fig 20 depicts the error caused by the linear approximation.

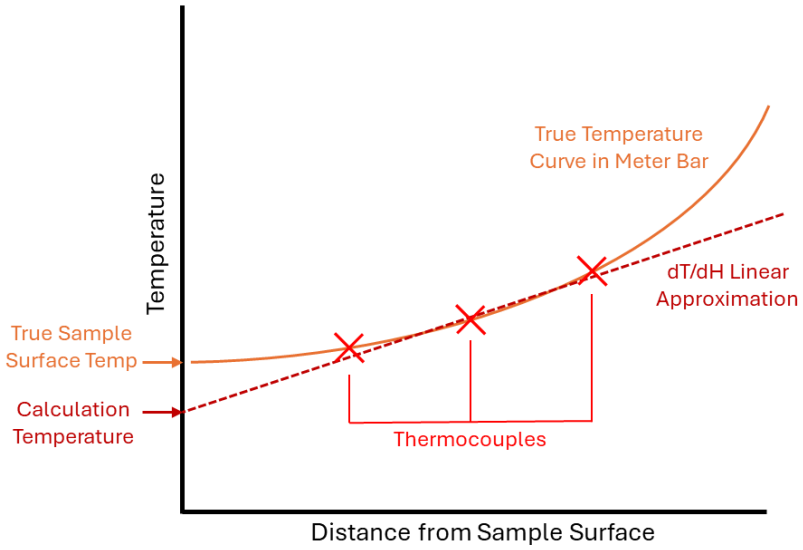

Fig. 20. Due to the thermocouple spacing, the linear approximation of the change in temperature in the meter bar (red) predicts a steeper drop in temperature than the true change in temperature (orange), leading to lower sample surface temperatures and greater calculated conductivity.

Use of thermistors or thermocouples with less noise along with spacing the thermocouples closer to the sample surface can improve the accuracy of thermal conductivity values. Additionally, while the improved system provides significantly less mistrials and much more usable data than the original setup, a considerable number of mistrials occurred. This can be attributed to inconsistent contact resistance between samples, distorting thermal conductivity calculations. Experimental data sets that yielded good values had a mean value of thermal interfacial resistance of 0.002609 $K \cdot m^2/W$ while those that generated bad results had resistances ranging from 0.0037 to 0.0103 $K \cdot m^2/W$. The thermal interfacial resistance between each set of trials can be compared using a control chart. Fig 21 presents an Individuals-Moving Range

control chart created from the resistances of the valid test trials, excluding one outlier (Ri = 0.0041 K·m²/W). All mistrial data sets except for one set exist outside of the upper control limit. When the contact resistance between the samples was inconsistent and the process was not in control, mistrials occurred and provided bad thermal conductivity data.

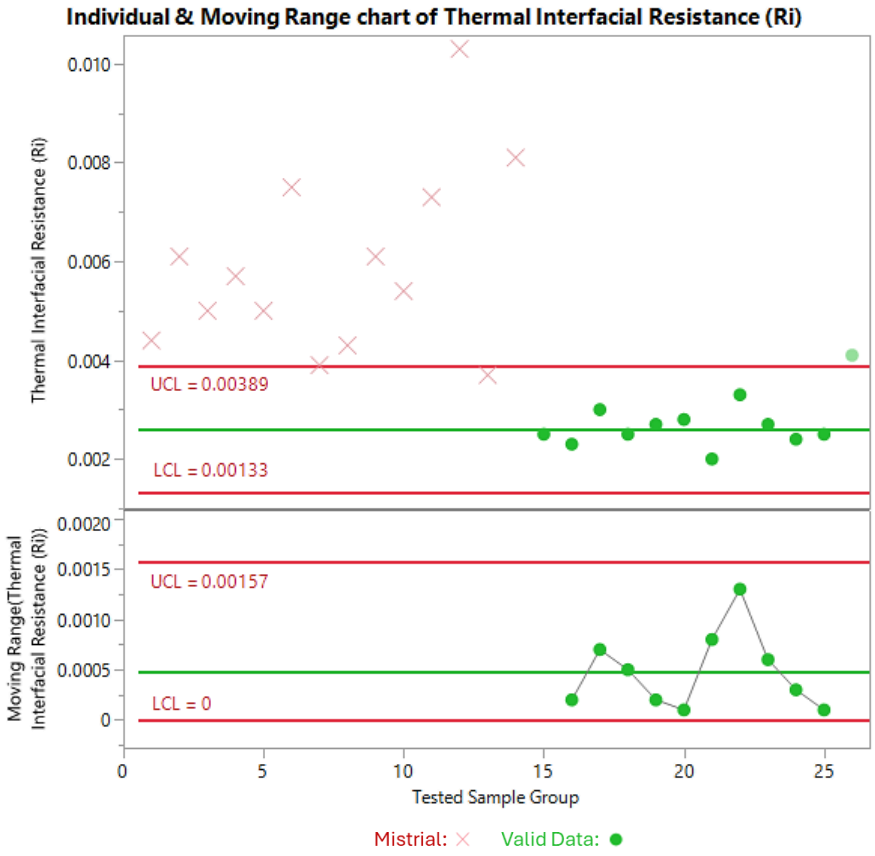

Fig. 21. Individual and moving range control chart of thermal interfacial resistance values for each set of trials. Nearly all valid data (green) contained Ri values in proximity to a mean of 0.002609 K·m²/W while the majority of mistrials (red) contained Ri values outside of the UCL.

Chapter 4: Experimental Results and Calculations

4.1 Experimental Data

Thermal conductivity data was obtained for longitudinal and transverse infill orientation samples of 10, 33, 55, 77, 92, and 100 percent infill densities created under the processing parameters discussed in section 2.3. The following are the experimental results summarized in table 4.

Table 4. Thermal conductivities of longitudinal and transverse orientation Onyx samples of increasing infill density.

Layup Direction	Infill Type	Infill Percentage	Thermal Conductivity (W/mK)
Longitudinal	Rectangular	10%	2.56
		33%	3.14
		55%	3.16
		77%	3.61
		92%	4.37
	Solid	100%	3.57
Transverse	Rectangular	10%	1.58
		33%	2.04
		55%	3.47
		77%	4.24
		92%	3.03
	Solid	100%	2.45

4.2 Example Calculations

Sample calculations outlining the process to obtain thermal conductivity values for the 55% infill transverse sample are shown below. From the experimental setup, temperature data is recorded for each thermocouple. After steady state has been reached ($\Delta T < 0.1$ ºC for 10 minutes), the average thermocouple reading over the ten-minute span is taken as the thermocouple temperature. An example of the collected trial data for the 10 mm sample is shown in table 5.

Table 5. Average steady state values for the 10mm 55% infill transverse heat flow trial.

Onyx 10 mm Transverse 55% Infill Sample			
Temperatures	**TC**	**Position (m)**	**Meter Bar**
25.304	-3	-0.035	Cold
25.481	-2	-0.020	Cold
25.549	-1	-0.005	Cold
64.268	1	0.005	Hot
65.353	2	0.025	Hot
65.361	3	0.045	Hot

From these values, a plot of thermocouple temperatures versus their position within the hot and cold meter bars is created with a linear regression fit. From this regression fit, dT/dH is determined from the slope and the sample surface temperature from the Y axis intercept for the hot and cold meter bar data. Fig 22 shows the evaluation of dT/dH and sample surface temperatures, which are summarized in Table 6.

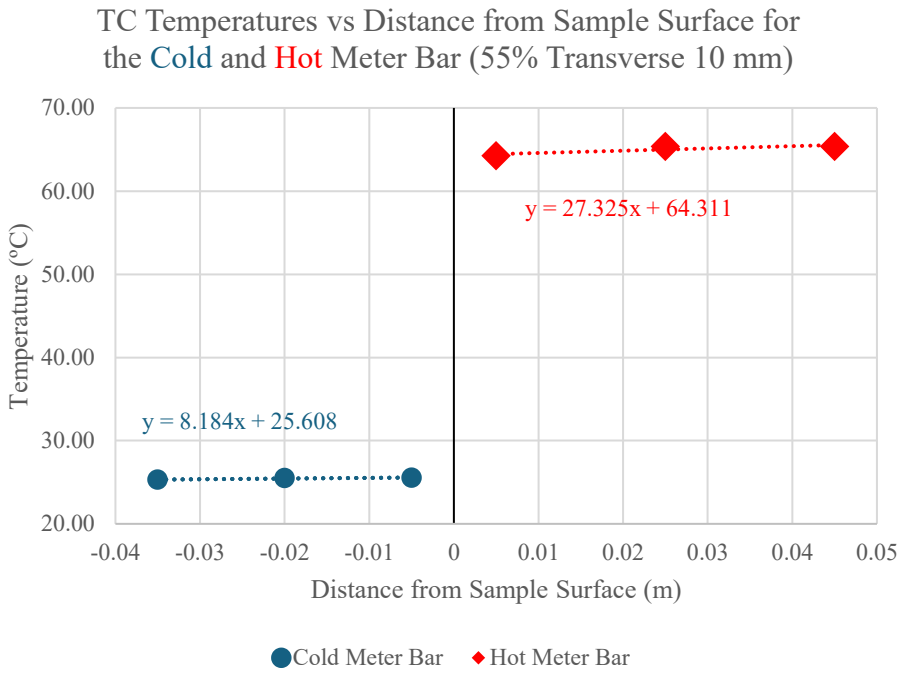

Fig. 22. Linear regression fits for hot and cold meter bar thermocouple data.

Table 6. Change in meter bar temperature and sample surface temperatures for hot and cold meter bars.

Meter Bar	**dT/dH**	**Surface Temperature (°C)**
Hot	27.325	64.311
Cold	8.184	25.608

From these values Q_{hot} , Q_{cold} are calculated using equation 2.4.1:

$$Q_{hot}\ (W) = \frac{dT}{dH} * A * Ref\ k \tag{2.4.1}$$

$$Q_{hot}\ (W) = 27.325\ \frac{°C}{m} * 0.002025\ m^2 * 390.8844 \frac{W}{mK}$$

$$Q_{hot}\ (W) = 21.629\ W$$

$$Q_{cold}\ (W) = \frac{dT}{dH} * A * Ref\ k$$

$$Q_{cold}\ (W) = 8.184\ \frac{℃}{m} * 0.002025\ m^2 * 390.8844 \frac{W}{mK}$$

$$Q_{cold}\ (W) = 6.478\ W$$

From the hot and cold meter bar heat flow, the average sample heat flow (Q) is taken as the average of both heat flow rates using equation 2.4.2:

$$Q(W) = \frac{Q_{hot} + Q_{cold}}{2} \tag{2.4.2}$$

$$Q(W) = \frac{21.629\ W + \ 6.478\ W}{2}$$

$$Q(W) = 14.054\ \mathrm{W}$$

Using the sample hot surface temperature (*Temp.H*), cold surface temperature (*Temp.C*), and the heat flow rate (*Q*), the thermal impedance for the sample is calculated (θ) using equation 2.4.3:

$$\theta\ \left(K * \frac{m^2}{W}\right) = \frac{A}{Q} * (Temp.H - Temp.C) \tag{2.4.3}$$

$$\theta\left(K * \frac{m^2}{W}\right) = \frac{0.0020025\ m^2}{14.054\ W} * (64.311℃ - 25.608℃)$$

$$\theta_{10\ mm\ sample} = 0.00558\ K * \frac{m^2}{W}$$

To offset for contact resistance, two samples of different heights were used for each data point. The thermal impedance of the 5 mm 55% transverse sample is also calculated using the previous methods. Its thermal impedance is given below:

$$\theta_{5\ mm\ sample} = 0.00414\ K * \frac{m^2}{W}$$

The true sample thermal conductivity (k_{sample}) is evaluated by calculating the rate of change between impedance and sample heights (h) and then taking the reciprocal of this value using equation 2.4.4.

$$k_{sample}\left(\frac{W}{mK}\right) = \frac{1}{\frac{\theta_{tall} - \theta_{short}}{h_{tall} - h_{short}}} \tag{2.4.4}$$

$$k_{sample}\left(\frac{W}{mK}\right) = \frac{1}{\frac{0.00558\ K*\frac{m^2}{W} - 0.00414\ K*\frac{m^2}{W}}{0.010\ \text{m} - 0.005\ \text{m}}}$$

$$k_{sample} = 3.47\,\frac{W}{mK}$$

Chapter 5: Thermal Conductivity Analysis

5.1 Transverse Sample Overview and Model

In general, test samples demonstrated a positive relationship between infill density and thermal conductivity. For samples of infill density from 10% to 77%, a linear relationship was observed with increasing infill density resulting in a proportional increase in thermal conductivity (0.0422 W/mK per 1% increase in infill). Higher infill density results in a greater number of infill channels extending from the hot to cold sample side and supports the proportional increase in thermal conductivity that occurs. COMSOL simulations for 33, 55, and 77% infill support this trend.

For infill density samples of 92% and 100% infill, a decrease in thermal conductivity was seen. After an infill of 77%, increasing infill density results in a decrease in thermal conductivity. The relationship between infill density and thermal conductivity is depicted in Fig 23. Table 7 presents a linear regression model for thermal conductivity of samples between 10 to 77% infill and a second linear regression model for the reduction in thermal conductivity experienced from 77 to 100% infill samples. These relationships can be used to model the thermal conductivity of a transverse heat flow sample of rectangular infill based on infill density.

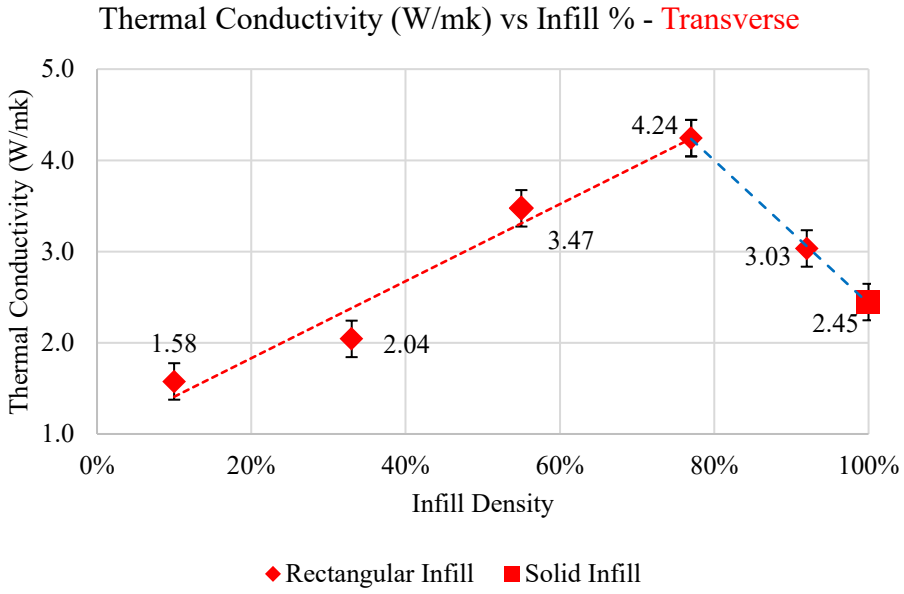

Fig. 23. Thermal Conductivity vs Infill Density for transverse samples of 10% to 100% infill.

Table 7. Regression fit models for thermal conductivity with respect to infill density (Infill%).

Fit Line	R Square	Equation
Linear Fit (10-77%)	0.963	$K\left(\frac{W}{mK}\right) = 0.9861394 + 4.2236242 * \text{Infill\%}$
Linear Fit (77-100%)	0.999	$K\left(\frac{W}{mK}\right) = 10.276 - 7.8449 * \text{Infill\%}$

For transverse heat flow, increasing infill density creates more infill channels in the heat flow direction, increasing thermal conductivity. However, at very high infill densities the parallel layered infill lines start intersecting and become interconnected along their lengths. This allows for heat transfer in the direction perpendicular to heat flow and therefore is likely responsible for the reduction in effective sample thermal conductivity. Fig 24 depicts the effects of increasing infill density.

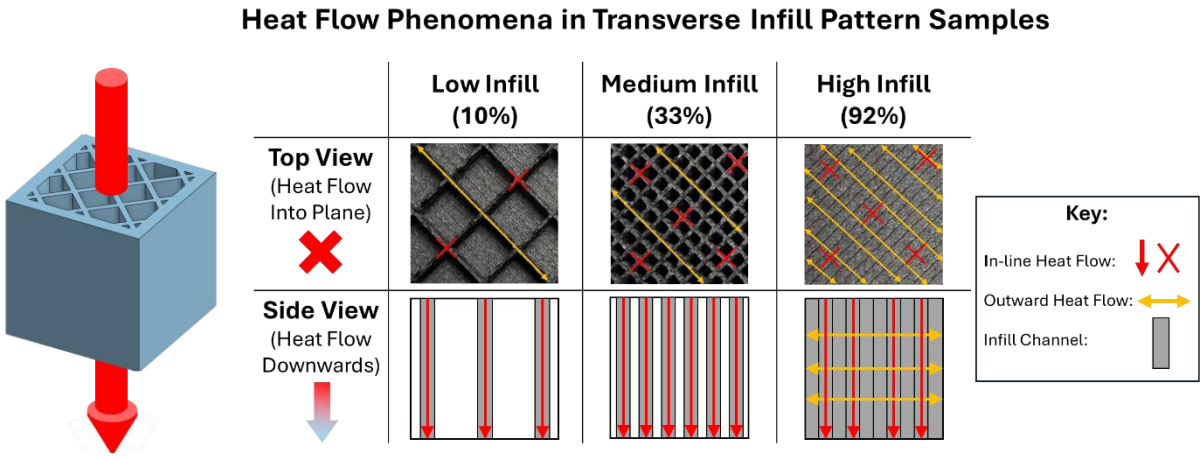

Fig. 24. Increasing infill results in increased thermal conductivity until interconnected infill layers result, promoting heat transfer away from the direction of system heat flow.

5.2 Longitudinal Samples Overview and Model

Longitudinal heat flow sample data also exhibited a positive relationship between infill density and thermal conductivity. Between infill densities of 10% to 92% there is a positive trend in thermal conductivity. COMSOL simulations for 33, 55, and 77% samples support this positive relationship. After 92% infill there is a reduction in thermal conductivity with increasing infill density, as seen in the case of the 100% infill sample having a reduced thermal conductivity. This trend is shown in Fig 25.

In the longitudinal direction increasing infill density adds more channels for heat to flow through from the hot to cold side. However, these infill channels are not parallel to the direction of system heat flow and are layered at 45-degree angles. Additionally, heat moving in the direction of system heat flow must pass through air pockets. With increasing infill density, the size of these pockets is reduced. Consequently, the number of pockets increases and requires heat to overcome a greater number of interfaces. Due to the more complex influence of these factors, thermal conductivity does not increase at a linear rate with increasing infill. Table 8 presents

linear and polynomial fit models for longitudinal sample conductivity. The linear fit does not represent the data as accurately as the polynomial model but is still relevant to show the positive relationship between infill density and conductivity. From the polynomial model the thermal conductivity of longitudinal samples can be predicted based on infill density between 10 to 92% infill.

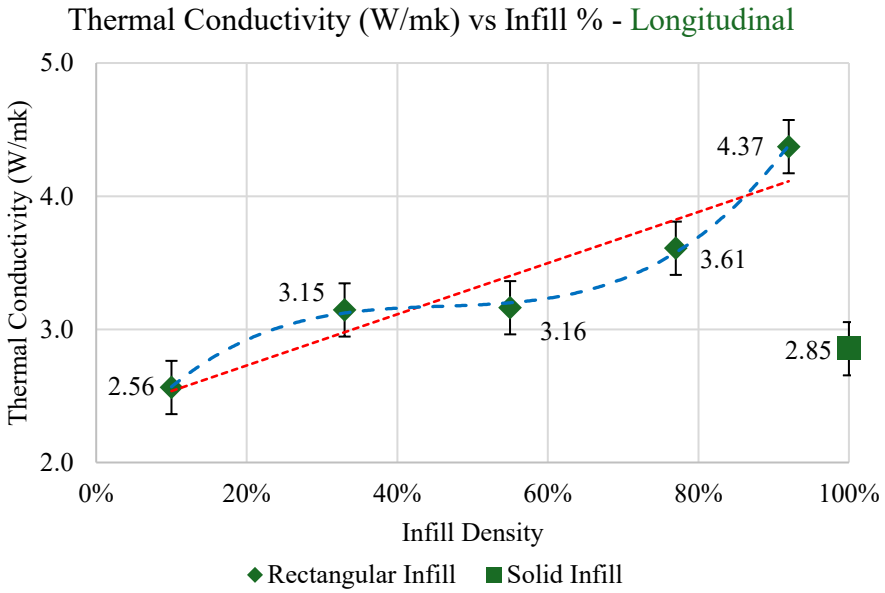

Fig. 25. Thermal Conductivity vs Infill Density for longitudinal samples of 10% to 100% infill.

Table 8. Regression analysis for longitudinal samples.

Fit Line	R Square	Equation
Linear Fit (10-92%)	0.889	$K\left(\frac{W}{mK}\right) = 2.3441741 + 1.9216214 * \text{Infill \%}$
Polynomial Fit (10-92%)	0.998	$K\left(\frac{W}{mK}\right) = 2.6358277 + 0.9938813 * \text{Infill\%} + 5.228422 * (\text{Infill\%} - 0.61167)^2 + 11.462805 * (\text{Infill\%} - 0.61167)^3$

Similar to the transverse samples, there is a decrease in thermal conductivity at high infill densities. At high infill densities the layered infill patterns begin to intersect and allow for heat to

transfer away from the direction of system heat flow. Unlike the transverse samples this phenomenon only had notable negative effects on effective conductivity at infill densities greater than 92% and was only seen for the 100% infill sample. Fig 26 depicts this effect.

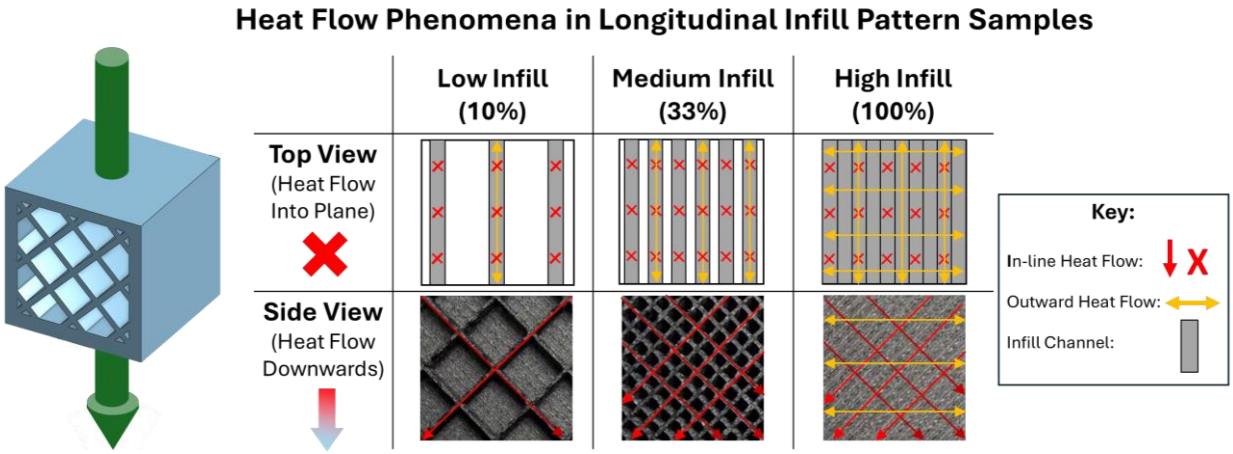

Fig. 26. For longitudinal samples, increasing infill raises conductivity until interconnected infill layers result, promoting heat transfer away from the direction of system heat flow.

5.3 Solid Infill Comparisons and Observed Phenomena

The transverse and longitudinal 100% infill samples showed differences in effective thermal conductivity. The longitudinal sample had a greater conductivity of 3.57 W/mK while the transverse sample was 2.45 W/mK. This difference is believed to be attributed to the angle of the carbon fibers with respect to heat flow.

Thermal conductivity of chopped fiber composite filaments is influenced by the fiber angle in respect to the direction of heat flow. Due to the effects of shear alignment during the extrusion process, the carbon fibers are generally aligned in the direction of the infill layup pattern deposition. For the solid infill samples this results in the longitudinal samples having layup and fiber directions at a 45-degree angle in the direction of heat flow. For transverse samples the infill layup and fiber direction are perpendicular to the direction of heat flow. Fig 27

illustrates the differences in carbon fiber angles in respect to heat flow. This results in longitudinal fibers making greater contributions to facilitating heat flow than the transverse samples since the fibers are closer in alignment with heat flow than the transverse sample.

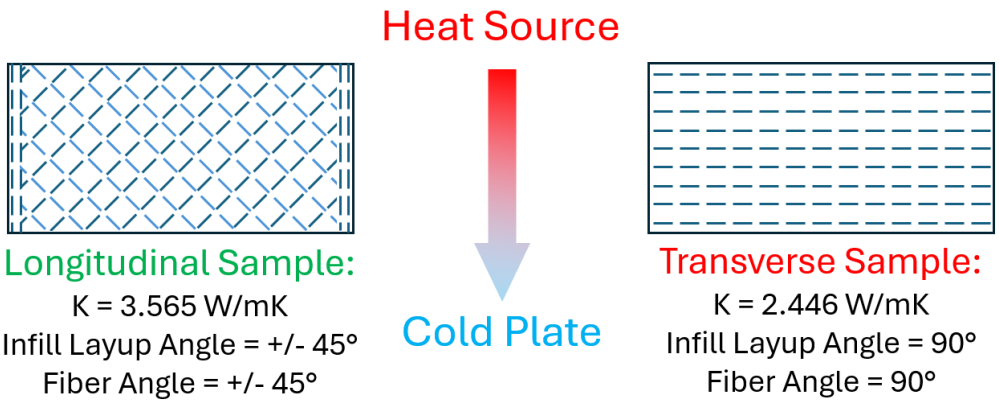

Fig. 27. Carbon fiber angles in respect to system heat flow for solid longitudinal and transverse samples. Angles closer to the direction of heat flow contribute to heat flow.

5.4 Low Infill Density Comparisons and Observed Phenomena

At the lowest infill density of ten percent, the longitudinal samples also exhibited greater thermal conductivity than the transverse samples. This is also believed to be the result of the carbon fiber angle with respect to heat flow. At ten percent infill the interior volume of the samples is for the majority air, and the infill material makes negligible contributions to heat transfer. For low infill samples most heat travels through the sample walls. For transverse samples the fiber angle within the walls and roof layers are perpendicular to the direction of heat flow due to being printed layer by layer from the sample floor to the roof. The longitudinal samples were printed at a 90-degree rotation, with the walls in contact with the base of the print bed. These samples were built by stacking layers from wall to wall. Therefore, when rotated back to the proper orientation for testing, the wall layup and fiber direction are in-line with the

direction of heat flow. This helps to facilitate more efficient heat flow and therefore results in higher effective thermal conductivity. Fig 28 shows the orientation of fibers within the walls of both samples.

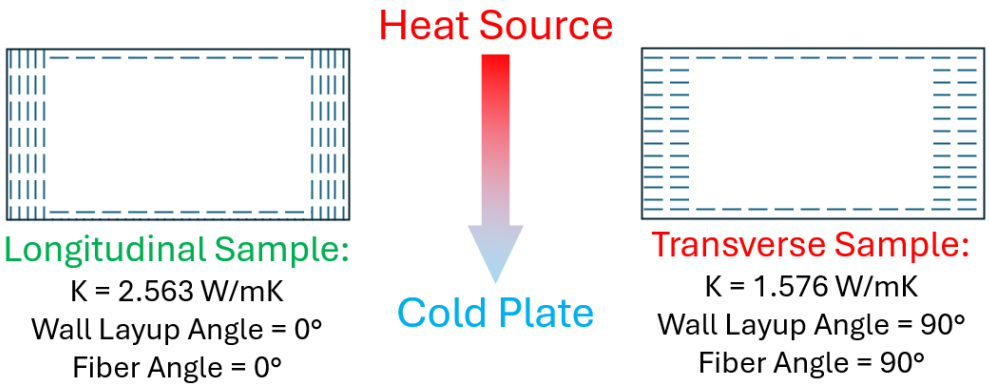

Fig. 28. Angles of CF in respect to system heat flow for low infill samples. Heat flow occurs mainly through sample walls. Fiber direction alignment in the walls promotes heat transfer.

5.5 Comparison of Reductions in Thermal Conductivity with High Infill Densities

As seen in Fig 23 and 25, longitudinal and transverse samples both experience a reduction in thermal conductivity at extremely high infill densities. However, the transverse samples see a much greater reduction than the longitudinal samples compared to their peak observed conductivity. Longitudinal samples saw an 18.5% decrease in thermal conductivity when comparing the 92 percent infill sample to the solid infill sample while transverse samples decreased in conductivity by 42.3% when comparing the 77 percent infill sample to the solid infill sample. Values of reduction are shown in Table 9.

Table 9. Maximum thermal conductivities and reductions from peak values with increased infill for longitudinal and transverse samples.

Layup Direction	Infill Percentage	Thermal Conductivity (W/mK)	Percent Reduction from Peak Value
Longitudinal	92%	4.37	-
	100%	3.57	18.5%
Transverse	77%	4.24	-
	92%	3.03	28.5%
	100%	2.45	42.3%

As previously discussed, the reduction in thermal conductivity is noticeable at high infill densities when interconnecting infill layers occur. This reduction is believed to be caused by the chopped fiber orientation in respect to system heat flow. Other studies have been performed evaluating the effects of infill density on thermal conductivity of printed pure thermoplastic samples with rectangular infill. From experimental results, no reduction in thermal conductivity occurred at high densities and only a positive relationship was seen [19]. The key differentiating factor between the thermoplastic filaments assessed by Tychanicz-Kwiecień et al and Onyx is the addition of chopped carbon fibers. Therefore, this difference in behavior can likely be attributed to their inclusion. In addition, this reduction may also be caused by the presence of trapped air pockets at higher infill densities.

Fiber direction of the infused carbon fiber strands likely plays a role in the more extreme degradation of effective thermal conductivity for the transverse samples. The carbon fibers have 96 times the thermal conductivity of the PA6 matrix they are imbedded within [14,15]. For transverse samples the fiber direction is perpendicular to the direction of heat flow and away from system heat flow. Therefore, when perpendicular heat flow is allowed, the fibers help facilitate outward heat flow due to their orientation in the same direction. Fig 29 illustrates this theory.

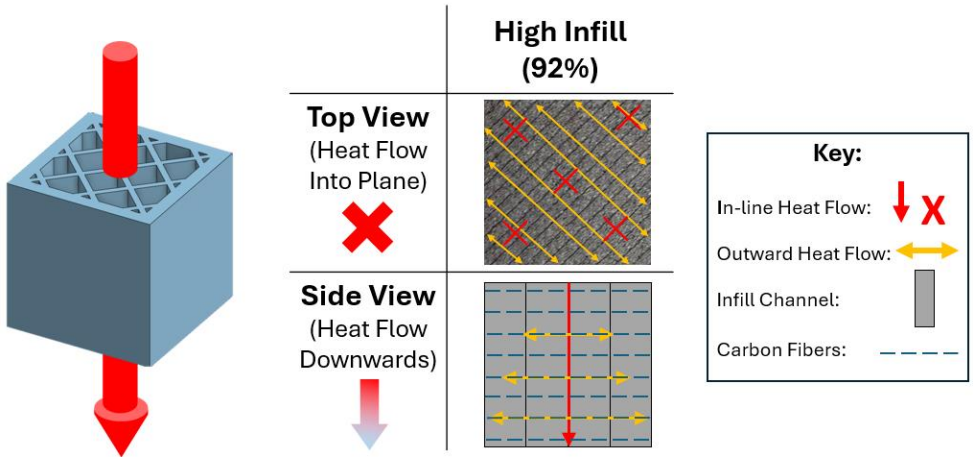

Fig. 29. For transverse samples when interconnecting infill channels occur, carbon fibers (blue) transverse to the direction of system heat flow (red) helps facilitate heat transfer outward (yellow).

A similar effect is seen in the longitudinal samples but to a lesser extent. The carbon fibers are aligned at a +/-45-degree angle in respect to system heat flow and contribute to outward heat flow. However, this angle is more aligned than the transverse fiber direction and therefore does not move heat outwards in its entirety and heat loss is not amplified as greatly. Fig 30 depicts the outward fiber heat flow.

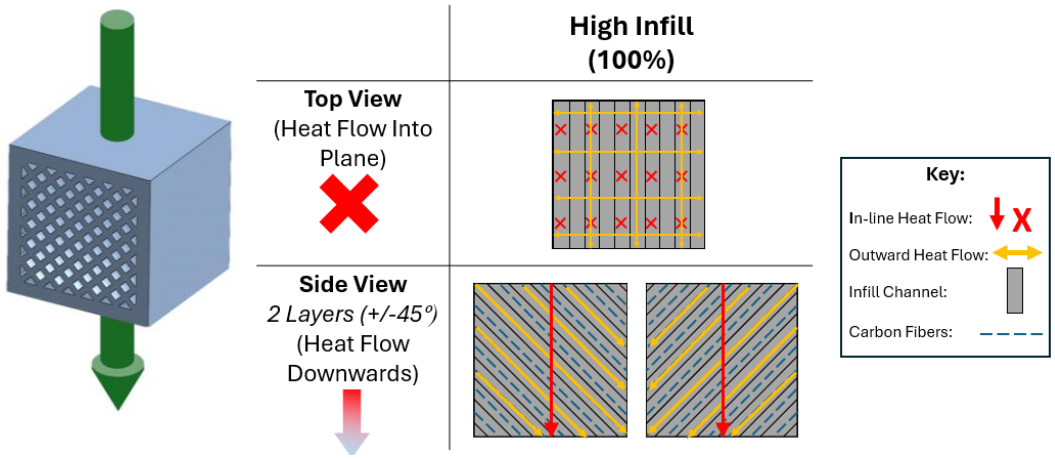

Fig. 30. Longitudinal samples similarly resulted in lower conductivity at infill densities with interconnecting infill layups occur. Less loss in thermal conductivity occurs than transverse samples due to carbon fibers (blue) being closer in alignment to system heat flow (red).

5.6 Highest Conductivity of Transverse and Longitudinal Samples

From the experimental data the highest thermal conductivity for transverse samples occurred at 77% infill density and for longitudinal at 92%, with conductivities of 4.24 and 4.37 W/mK, respectively. For transverse samples 77% infill is the highest tested infill density that did not result in parallel laid up infill layers coming into contact and therefore provides the highest number of channels linking the hot and cold sample sides without promoting heat transfer outwards from the direction of system heat flow. For longitudinal samples, the 92% infill density provided the most optimum ratio of infill to size of air pockets without fully interconnecting infill deposition lines. While some connection between parallel infill layers occurred, having fiber angles only 45 degrees off from the direction of system heat flow provided a less detrimental effect to overall system heat flow. This loss is compensated for by nearly eliminating the air pockets and adding more infill channels. Heat flow for the most optimal infill densities are shown in the figure below.

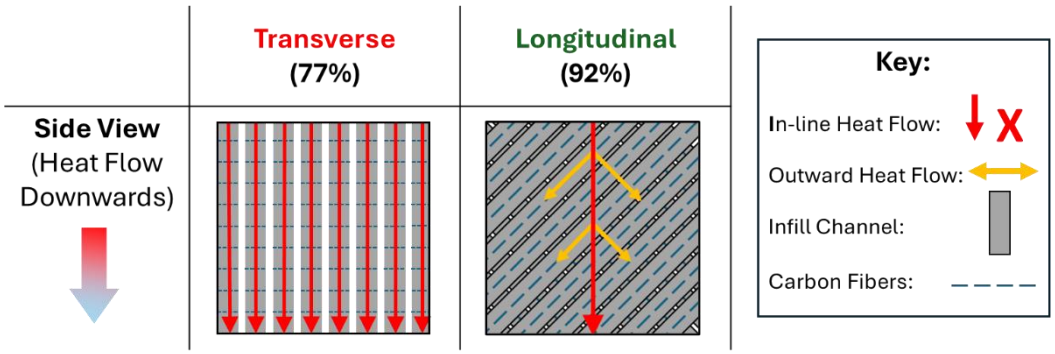

Fig. 31. Comparison of heat flow through highest thermal conductivity transverse and longitudinal samples with respect to infill geometry and carbon fiber direction.

The differences between the highest thermal conductivity for the longitudinal and transverse samples only showed a difference of 0.129 W/mK greater for the longitudinal sample and does not exhibit a significant difference. In theory, the transverse geometry should be superior as it provides more channels in the direction of system heat and are not disrupted by air pockets that intersect system heat flow. The longitudinal samples do not contain infill paths parallel to the direction of system heat flow and additionally have disrupting air pockets. This less efficient geometry for heat transfer is balanced by having the chopped carbon fibers more closely aligned with the direction of heat flow, as they contribute much more to the thermal conductivity of the Onyx filament than the PA6 matrix.

5.7 Importance of Chopped Carbon Fiber Angle in Composite Thermal Conductivity

In composite materials the angle of the reinforcement fibers has a profound impact on mechanical properties. For mechanical properties, this is referred to as a Krenchel or efficiency factor, as the orientation of the reinforcement fibers in relation to the applied load effects mechanical properties with higher alignment resulting in greater properties. A similar phenomenon is present for thermal properties of a material. In carbon fiber laminates with

continuous fibers, thermal conductivity is influenced by the fiber angle in respect to heat flow, with thermal conductivity degrading with further alignment from the direction of heat flow.

In a study conducted by Bao et al, thermal response of carbon fiber laminates with different fiber angles was studied. According to their experimental results, thermal resistance of samples with fibers angled 90-degrees from system heat flow were nearly double the thermal resistance of 45-degree sample orientations, with resistances of 5.000 K/W and 2.563 K/W, respectively [20]. While their study was conducted with continuous fiber composites and the exact numerical difference in resistance is likely not applicable, the same relationship of increased alignment resulting in greater thermal conductivity can be applied to chopped fiber carbon fiber composites.

The influence of the carbon fiber angles has a major influence on sample thermal conductivities as even with a less efficient geometry for heat transfer, the longitudinal samples have a similar maximum recorded conductivity to transverse samples due to more aligned fiber direction. Greater fiber alignment with heat flow allows low and high infill longitudinal samples to exceed transverse sample conductivities.

Similar to other studies testing pure thermoplastic FDM printed materials, increasing infill density raises thermal conductivity [19]. However, the reduction at high infill densities does not exist in pure thermoplastic filaments, as interconnected infill layers likely do not detract from effective thermal conductivity as there are no high conductivity fibers extending in the directions outwards from heat flow.

Chapter 6: Finite Element Analysis Comparisons

6.1 COMSOL FEA Simulation of Experimental Setup

Finite Element Analysis (FEA) was implemented to analyze the trends between infill density and heat flow direction on thermal conductivity. COMSOL Multiphysics was used to simulate a simplified hot meter bar experimental setup. The simulated test samples were 10 x 10 x 10 mm samples of 33, 55, and 77 percent infill density for both the longitudinal and transverse infill orientations. The samples were placed between 2 copper meters bars of equivalent dimensions and a programmed thermal conductivity of 400 W/mK to model the experimental setup's copper meter bar material. A constant heat rate of 20 Watts was applied to the top surface of the top meter bar to simulate the cartridge heater. A convective heat flux of 25 W/m^2K was applied to the bottom surface of the lower meter bar to simulate the effects of the recirculating cooler. Heat flow simulation was performed for an experiment time of 10,000 seconds (2.78 hours) to ensure steady state heat flow was achieved. At the 10,000 second mark, the sample surface temperatures (*Temp.H, Temp.C*) and change in temperature in the meter bar (*dT/dH*) were obtained to compute the thermal conductivity of the sample. The following equations were used to calculate thermal conductivity of the sample.

$$Q(W) = \frac{dT}{dH} * A * Ref\ k \tag{6.1.1}$$

$$k_{sample}\left(\frac{W}{mK}\right) = \frac{Q*\mathrm{h}_{sample}}{\mathrm{A}*(\mathrm{Temp.H} - \mathrm{Temp.C})} \tag{6.1.2}$$

Only one sample height per data point was needed due to a lack of contact resistance in the simulation. The sample material was set to the estimated thermal conductivity of Onyx at 5.00 W/mK, which is discussed in further detail in section 7.1.

The simulated material differed from Onyx as the material contained isotropic thermal properties and was not a chopped fiber composite with varying fiber angles. While unable to accurately simulate the fiber angle phenomena observed, the simulation was used to understand the effects of the geometry itself on thermal conductivity and to determine if there is support for a positive relationship between infill density and thermal conductivity. For simplification of analysis, convection through the air channels within the infill pattern were ignored as their contribution to thermal conductivity is negligible compared to the Onyx material. Figure 32 shows the simulated hot meter bar setup with a heat map at the simulation time of 10,000 seconds. Fig 33 plots example simulation temperature data results from which surface temperature and meter bar dT/dH data was gathered.

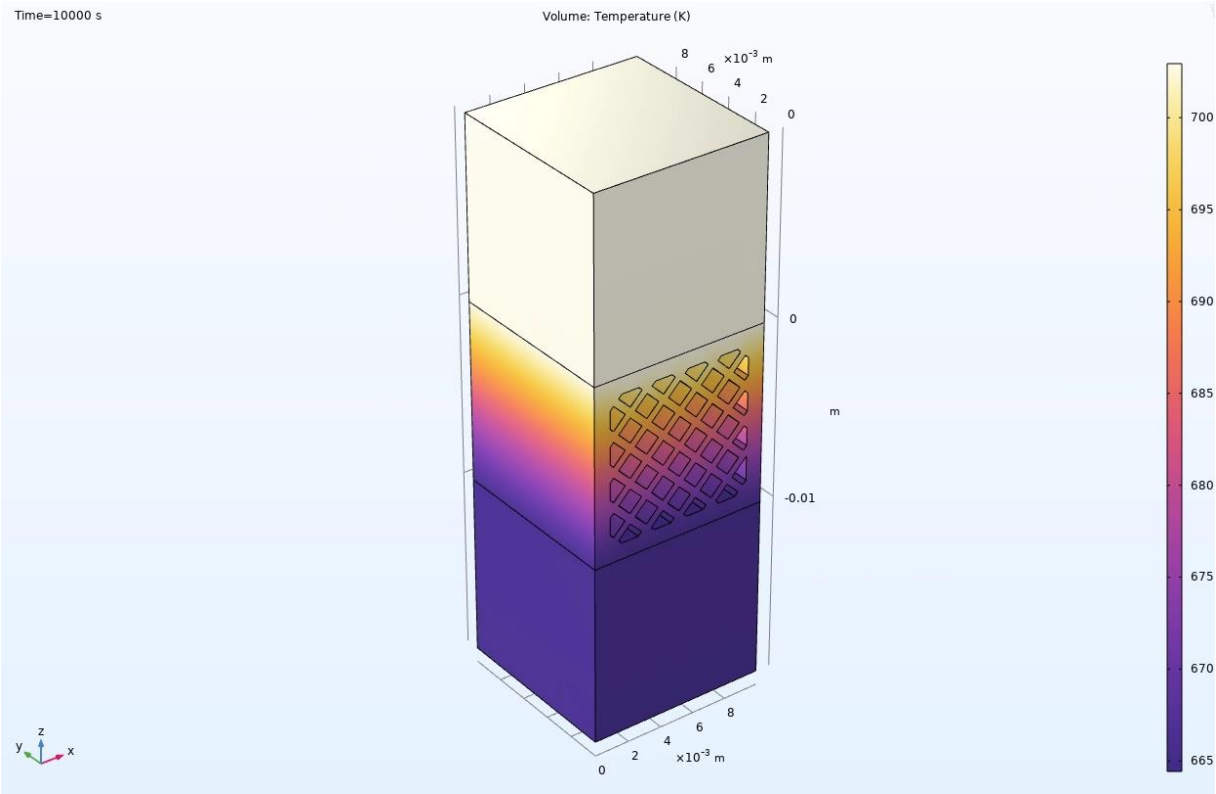

Fig. 32. COMSOL simulation of meter bar setup testing 55% Longitudinal sample.

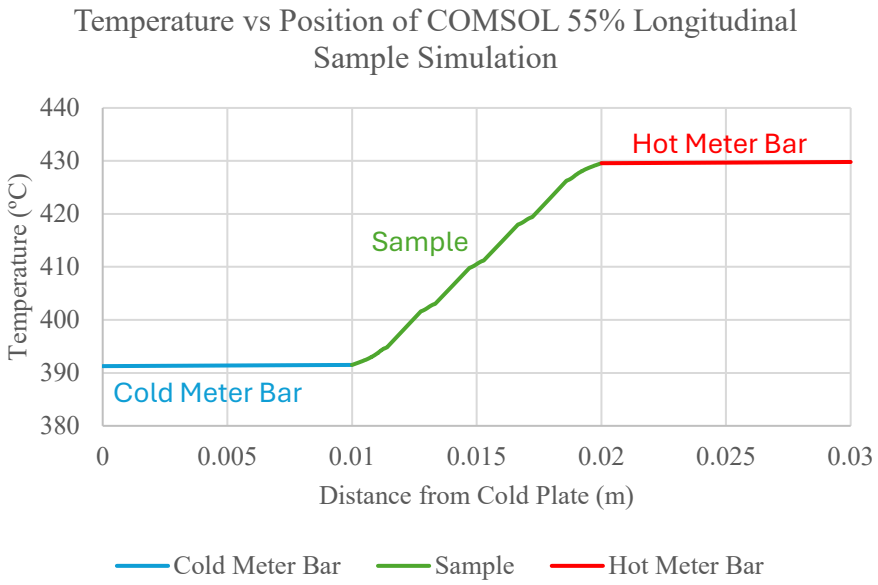

Fig. 33. COMSOL temperature data for 55% longitudinal sample simulation.

6.2 Calculations for Simulation Conductivity and Impedance

For each simulated sample calculations were performed to evaluate the thermal conductivity and impedance to compare simulation trends. Conductivities were evaluated through the following outlined method.

First the heat flow rate (Q_{Sample}) is calculated using the rate of change in temperature within the sample (dT/dH), the sample surface area (A), and the simulated meter bar thermal conductivity ($Ref\ k$).

$$Q_{Sample}\ (W) = \frac{dT}{dH} * A * Ref\ k \tag{6.2.1}$$

Fourier's law is used to calculate the sample thermal conductivity ($K_{Simulated}$) from the heat flow rate, change in temperature (ΔT) between the sample faces, and the sample length (l).

$$K_{Simulated}\ (W/mK) = \frac{Q_{Sample} * l}{A * \Delta T} \tag{6.2.2}$$

Simulated thermal impedances are calculated using temperature changes, sample heat flow rate, and the sample surface area.

$$\theta\left(\frac{K*m^2}{W}\right) = \frac{A}{Q} * (Temp.H - Temp.C) \tag{6.2.3}$$

The following are example calculations for the simulated longitudinal 33% infill sample:

$$Q_{Sample}\ (W) = \frac{dT}{dH} * A * Ref\ k \tag{6.2.1}$$

$$Q_{Sample}\ (W) = 18.41\text{K/m} * 0.0001\ m^2 * 400\,\frac{W}{mK}$$

$$Q_{Sample}\ (W) = 0.736\ W$$

$$K_{Simulated}\ (W/mK) = \frac{Q_{Sample}*l}{A*\Delta T} \tag{6.2.2}$$

$$K_{Simulated}\ (W/mK) = \frac{0.736\ W * 0.010\ m}{0.0001\ m^2 * 51.07\ ºC}$$

$$K_{Simulated}\ (W/mK) = 1.442\ W/mK$$

$$\theta\left(\frac{K*m^2}{W}\right) = \frac{A}{Q} * (Temp.H - Temp.C) \tag{6.2.3}$$

$$\theta\left(\frac{K*m^2}{W}\right) = \frac{0.0001\ m^2}{0.736\ W} * (51.07\ ºC\ )$$

$$\theta\left(\frac{K*m^2}{W}\right) = 0.00694\ (K*m^2)/W$$

6.3 Simulation Thermal Conductivity Results

Below is a summary of COMSOL simulation results in Table 10 and a comparison of thermal conductivities between orientations and infill densities in Fig 34. Conductivity values were calculated using the methods outlined in section 6.2.

Table 10. COMSOL results for 33, 55, and 77 percent infill longitudinal/transverse samples.

Layup Direction	**Infill Percentage**	**Simulated Conductivity (W/mK)**	Change in Temp.(ºC)	DT/DH	Heat Flow Q (W)	Thermal Impedance (K*m²)/W
Longitudinal	33%	1.442	51.07	18.41	0.736	0.0069
	55%	2.135	38.07	20.32	0.813	0.0047
	77%	2.893	29.46	21.31	0.852	0.0035
Transverse	33%	4.193	34.57	36.24	1.450	0.0024
	55%	4.681	28.19	32.99	1.320	0.0021
	77%	4.711	23.95	28.21	1.129	0.0021

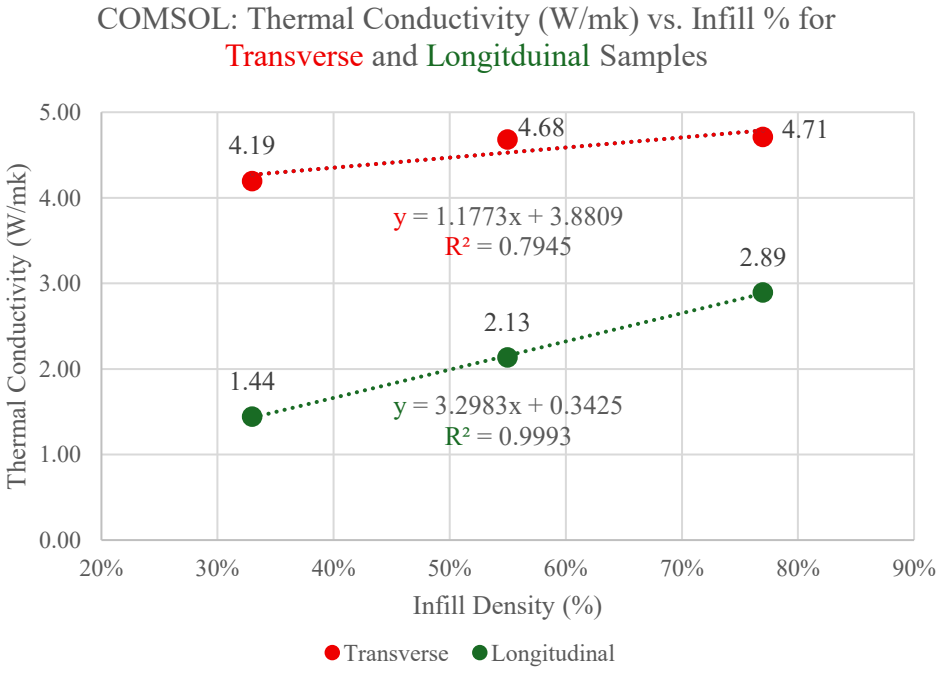

Fig. 34. Thermal conductivity vs infill density for longitudinal and transverse COMSOL simulation samples.

Simulation results show that for longitudinal and transverse samples there is a positive relationship between infill density and thermal conductivity for infill densities between 33 and 77%. The simulation analysis supports the experimental data's positive trends between thermal conductivity and infill density. When comparing the infill geometry through simulation results, the transverse geometry is much more efficient facilitating heat transfer and exhibits roughly twice the thermal conductivity of its longitudinal counterparts. The transverse samples from the experimental data did not exhibit this disparity, as the longitudinal samples were within a similar range of thermal conductivity values. However, longitudinal samples from real experimental data have carbon fibers at a 45-degree angle in respect to system heat flow while transverse samples have fibers perpendicular to heat flow. According to Bao et al, thermal resistance for fibers in the perpendicular direction to heat flow is nearly double that of fibers at a 45-degree offset [20]. Therefore, fiber angles of the experimental samples are likely what allow the longitudinal thermal conductivities to reach and exceed those of the transverse samples.

Chapter 7: Rule of Mixtures Estimates and Traditional Laminate Composite Comparisons

7.1 Rule of Mixtures (ROM) Estimates for Onyx Thermal Conductivity

Onyx filament is a composite chopped fiber filament containing an 80% to 20% volumetric ratio between its PA6 and Carbon Fiber constituents [2,3]. PA6 has a thermal conductivity of 0.25 W/mK [17] and graphite carbon fibers have a thermal conductivity 24 W/mK [18].

Through Rules of Mixtures (ROM) principles, the theoretical maximum thermal conductivity with fiber alignment in the direction of heat flow can be estimated. This calculation is performed using the volumetric ratios of PA6 (*Vm*), the carbon fibers (*Vf*), and their individual thermal conductivities (*km, kf*) [21]. Calculations are shown below.

$$Upper\ Limit\ \ kC = Vm * km + Vf * kf \tag{7.1.1}$$

$$Upper\ Limit\ kC = (0.8) * (0.25\ W/mK) + (0.2) * (24\ W/mK)$$

$$Upper\ Limit\ kC = 5.00\ W/mK$$

The estimated thermal conductivity of Onyx is 5.00 W/mK. This number aligns with Onyx thermal conductivity estimates from Inan's work of 5.111 W/mK [6]. The highest recorded experimental thermal conductivity was 4.37 W/mK for the 92% longitudinal sample. Implementing the proposed correction factor to compensate for system inaccuracy adjusts this value to 3.419 W/mK. Both experimental and corrected values are within the estimated maximum.

The ROM estimate assumes perfect fiber alignment along the direction of heat flow. In the 92% infill longitudinal sample the fibers are 45 degrees offset from system heat flow and will not be as efficient. Therefore, a lower maximum observed thermal conductivity within proximity of the estimated maximum confirms experimental results and validates the estimated Onyx thermal conductivity.

7.2 Transverse Heat Flow Comparison to Traditionally Manufactured Composites

The thermal conductivity of Onyx was compared to traditionally manufactured carbon fiber composite laminates. Carbon fiber samples were created of the same length and width as the experimental samples (1.8 in x 1.8 in) with thicknesses of 0.125 and 0.25 inches (3.175 and 6.35 mm). The carbon fiber sheet was sourced from McMaster Carr (PN: 8181K16). This carbon fiber laminate sheet combines 3k plain weave carbon fiber fabric with 0/90-degree orientations embedded within a prepreg epoxy resin. The fiber volume fraction is 57.6% fiber and 42.3% resin [22]. Samples were cut from sheets using a Proto MAX abrasive waterjet.

Carbon fiber sheet samples were tested in the transverse heat flow direction perpendicular to the planes of each laid up carbon fiber sheet. The resulting thermal conductivity was 1.32 W/mK. Multiple publications have evaluated transverse heat flow through carbon fiber laminates with epoxy resin matrices and have determined that laminates with fiber volumetric fractions between 50 to 70 percent exhibit a range of thermal conductivities from approximately 0.9 to 1.25 W/mK [23]. With the system correction factor the corrected measured thermal conductivity is 1.03 W/mK, which is within the literature values. The proximity of the experimental values to recorded literature values confirms validity of the experimental data. Fig 35 provides a comparison of carbon fiber sheet conductivity compared to the highest thermal conductivity Onyx sample and the 100 percent infill sample for transverse heat flow.

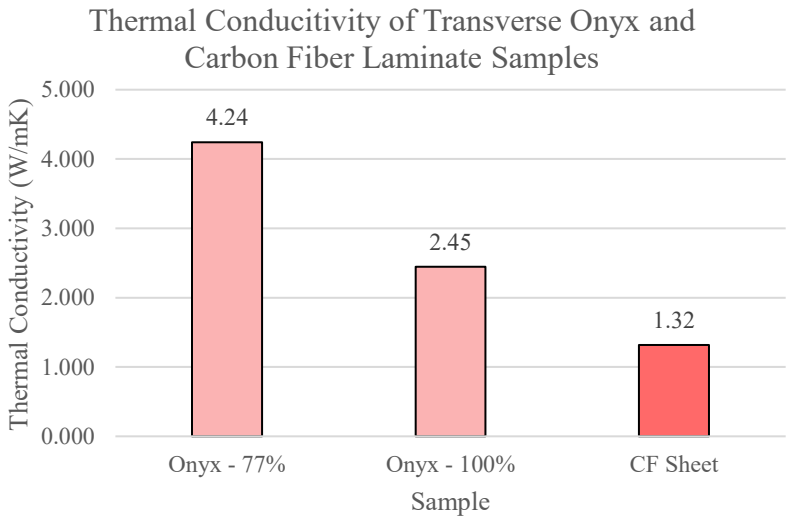

Fig. 35. Comparison of Onyx and Carbon Fiber sheet transverse thermal conductivities.

The onyx samples exhibit considerably higher thermal conductivity than the laminated carbon fiber sheet. The solid infill sample has an 85.6% greater thermal conductivity than the laminate sheet and the highest conductivity transverse sample is 221.9% greater. The Onyx 77% infill sample's geometry promotes heat transfer much more efficiently than alternating stacked interfaces of carbon fiber weave and epoxy. At 100% infill the thermal conductivity is reduced from the previously discussed phenomena of connected infill layers promoting heat transfer outwards through the carbon fibers in the direction perpendicular to system heat flow.

The carbon fiber sheets provide more evidence for this theory. From volumetric ratios of the laminate sheet, the theoretical maximum thermal conductivity should be equivalent to 13.92 W/mK and significantly greater than any of the onyx samples due to its 2.88 times greater ratio of carbon fibers. However, since the fibers are arranged perpendicularly to the direction of system heat flow, effective thermal conductivity is greatly reduced as the fibers facilitate heat transfer outwards. Compared to the FDM printed samples, this effect is amplified for the carbon fiber sheet as the carbon fibers are continuous and connected within each layer of the laminate

and are at a higher volumetric ratio than the epoxy. Fig 36 shows the differences in heat flow between the laminate samples and onyx samples in transverse heat flow due to fiber effects.

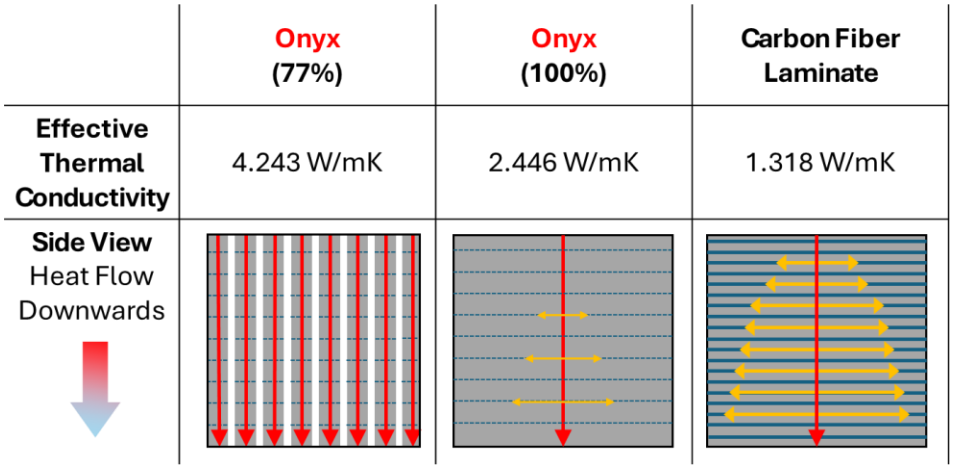

Fig. 36. For laminate samples, increasing carbon fiber volume content and continuous fibers increase heat transfer away from the direction of transverse heat flow, reducing effective thermal conductivity.

Chapter 8: Results, Conclusions, and Future Work

8.1 Overview of Experimental Results

For both longitudinal and transverse heat flow directions, increasing infill density results in higher thermal conductivity up until a density is reached where parallel infill layers became interconnected. Transverse samples have a strong positive linear relationship with infill density and thermal conductivity for densities up to the point of intersecting infill layers (77%). Raising infill density results in a proportional increase in infill channels in the direction of heat flow. In other studies, pure thermoplastic FDM printed samples with rectangular infill patterns experience similar trends. For PLA, PET-G, and ABS samples a positive linear relationship is seen for transverse heat flow for sample infill densities from 40% to 80%, supporting experimental results [19].

Longitudinal samples have a weaker but still positive linear relationship between infill density and thermal conductivity up to the point of heavily intersecting infill layers (92%). The relationship's linearity is weaker than the transverse samples due to the more complex geometry in the direction of system heat flow, involving air pocket interfaces and infill channels at an angle offset from system heat flow.

At high infill densities there is a reduction in effective thermal conductivity. For transverse samples this phenomenon becomes noticeable after approximately the 77% infill region and for longitudinal samples near the 92% infill region. Solid infill samples did not have the maximum thermal conductivity of the experimental densities. At 100% infill, longitudinal samples exhibit greater thermal conductivity than transverse samples.

Low infill results in low thermal conductivity. Transverse samples with low infill density provide optimal insulation. For both orientations, the greatest amount of infill density until the point of interconnecting infill layers is reached (Transverse – 77%, Longitudinal – 92%) results in the highest thermal conductivity. Fig 37 summarizes the experimental data from this study.

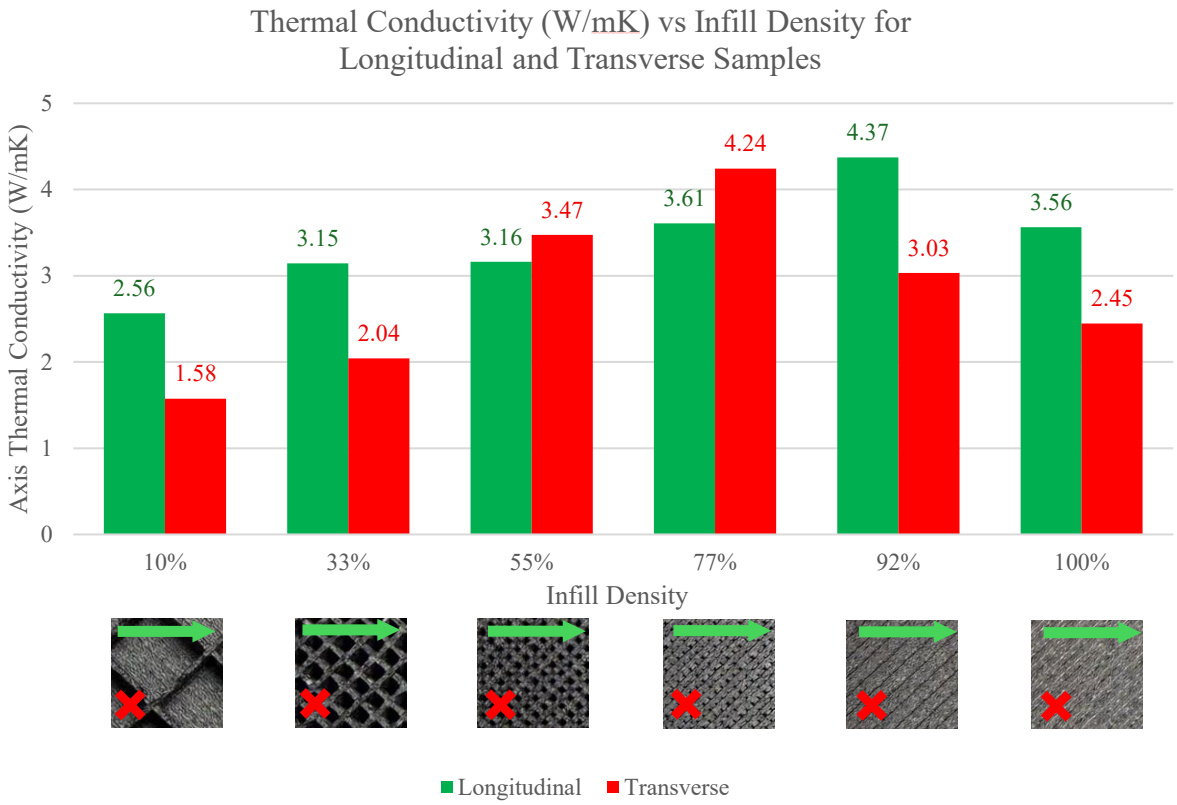

Fig. 37. Overall summary of experimental data. Comparison of longitudinal and transverse thermal conductivity with increasing infill density.

8.2 Influence of Chopped Fibers and Orientation on Thermal Conductivity

The thermal conductivity of the Onyx filament is primarily influenced by the chopped carbon fiber strands. While only 20% of the volume of the material is carbon fiber, it dictates the majority of the filament's conductivity. The fibers are 96 times greater in thermal conductivity than the PA6 matrix they are embedded within. From the rule of mixture estimates, it can be

determined that 96% of the Onyx thermal conductivity is from the carbon fibers (4.8 W/mK out of 5.0 W/mK).

The orientation of the chopped fibers in respect to system heat flow has a significant impact on the effective thermal conductivity. In other literature the thermal conductivity of chopped carbon fiber composite materials has been examined. Extruded HDPE composite samples were noted to increase their effective thermal conductivity with greater chopped fiber alignment in the direction of system heat flow [24]. While not for FDM printing purposes, extruded HDPE composite samples are analogous to the FDM extrusion process and should exhibit similar behaviors. An applicable takeaway from the work of Kang et al is that chopped carbon fibers facilitate heat flow and increase thermal conductivity along the direction of their alignment.

In the FDM printing process the chopped fibers are generally aligned in the direction of print layup due to the effects of shear alignment during filament extrusion [25]. Therefore, the infill layup direction and pattern determine the orientation of the chopped fibers. For longitudinal samples this results in fibers within the infill pattern at a +/- 45-degree difference to the direction of heat flow while the fiber direction in the walls is parallel to heat flow. For transverse samples the infill layup and fiber direction is perpendicular to system heat flow for both the walls and infill region. This results in the longitudinal infill fibers making greater contribution to heat flow than the transverse sample fibers due to greater fiber alignment with system heat flow, raising effective thermal conductivity. Fig 38 shows the fiber angles within each sample and their impacts.

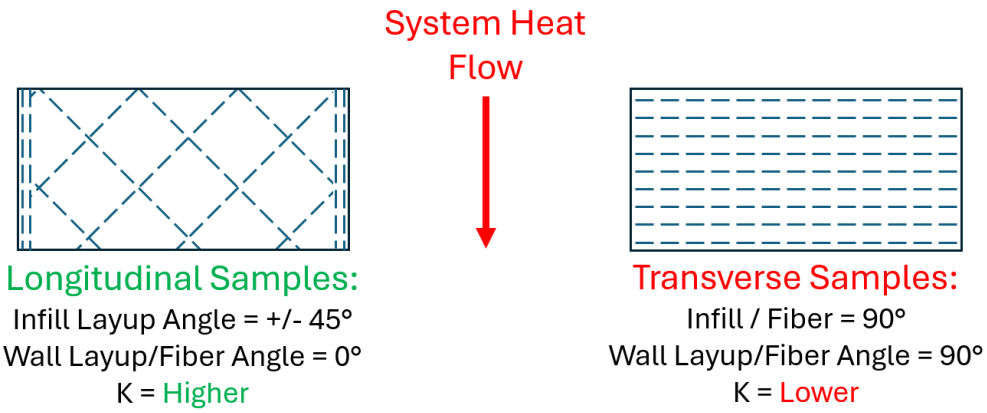

Fig. 38. Effective thermal conductivity is primarily influenced by the angle of fibers with respect to heat flow. While the transverse samples had a more thermally efficient geometry, they were unable to supersede the effects of greater fiber alignment in the longitudinal samples.

The orientation of fibers in continuous fiber composites having major influence on effective thermal conductivity is well documented in literature [20] [26]. Even though from simulation results the transverse infill geometry should show much greater effective thermal conductivity than the longitudinal samples, the fiber orientation compensates for the geometry. This allowed longitudinal conductivities to exceed transverse values for the majority of tested sample densities.

The phenomenon of extremely high infill densities lowering effective thermal conductivity is believed to be facilitated by fibers as well. In pure thermoplastic studies, increasing infill density never causes a reduction in effective thermal conductivity at high density [19]. From sample infill cross sections, it was seen that at high infill densities the parallel layered infill segments begin to interconnect. From the results of this study, it is theorized that the interconnecting infill layers allows heat to transfer between infill layers and flow outwards through the fibers angled away from the direction of system heat flow. Samples with fiber angles in the perpendicular direction to heat flow accentuate this phenomenon as they allow heat

travelling through intersecting layers to travel more efficiently away. Transverse samples saw a greater reduction in conductivity than longitudinal samples due to having fibers perpendicular to heat flow. This phenomenon is also exhibited by the fact that the carbon fiber laminate samples with higher volumetric ratios of carbon fibers with orientation perpendicular direction to transverse heat flow resulted in lower effective thermal conductivities than all tested onyx samples. This reduction is seen in literature as well as experimental values and is significantly lower in conductivity than heat flow along the direction of the carbon fibers [23]. Additionally, the less efficient heat transfer between high infill density samples may be due to the presence of trapped air pockets.

8.3 Conclusions and Takeaways

Compared to pure plastic prints, the inclusion of chopped carbon fibers within a composite filament greatly increases the thermal conductivity of the material. From experimental results it can be concluded that increasing infill density for samples of both heat flow directions will increase the effective thermal conductivity until a great enough infill density is reached where parallel infill layers begin to connect. Due to these effects, solid infill samples will not have the greatest thermal conductivity unless the fibers are oriented towards the direction of heat flow.

For transverse samples there is a positive relationship between infill density and thermal conductivity from 10% to 77% sample densities. For longitudinal samples there also exists a positive relationship for infill densities between 10% to 92%. The greatest thermal conductivity before reduction occurs is around 77% infill for transverse samples and approximately 92% for longitudinal samples. These values can be used to maximize thermal conductivity of prints. From all tested samples, the highest thermal conductivity was achieved by longitudinal samples of

92% infill density. To maximize insulation, the lowest infill density possible will result in the lowest conductivity. In this study the lowest density was 10% infill for both sample types with transverse samples yielding the lowest recorded value.

The Onyx filament thermal conductivity is heavily influenced by the chopped carbon fibers, as they are significantly greater in conductivity than the PA6 matrix they are embedded within. Due to effects of shear alignment during FDM filament extrusion, the fibers are aligned with the direction of material layup during printing. The orientation of these fibers in respect to the direction of heat flow has a profound effect on the thermal conductivity, as greater alignment improves thermal conductivity while further disparity between the fiber and heat flow angle reduces thermal conductivity.

The transverse orientation is more efficient for heat transfer than the longitudinal orientation due to the interior infill geometry providing channels parallel to the direction of heat flow without intersecting air pockets. FEA simulations support this theory. However, the chopped fiber orientation within these channels is perpendicular to heat flow while for longitudinal samples it is at a 45-degree offset. Additionally, longitudinal samples have parallel fibers within the walls. This greater fiber alignment in longitudinal samples allows their thermal conductivity to be in proximity and to even exceed transverse conductivities at extremely low and solid infill densities.

In theory, the chopped fibers are believed to be responsible for the reduction in thermal conductivity seen at high infill densities. Since the fibers increase thermal conductivity when aligned with system heat flow, they likely facilitate heat transfer away from system heat flow if their fibers are aligned incongruently. When infill layers at high densities interconnect, they promote outward heat transfer through fibers oriented away from the direction of system heat

flow. This theory is supported by the laminate carbon fiber sample. This sample with the highest volumetric ratio of carbon fibers in the transverse fiber orientation resulted in the lowest recorded thermal conductivity of all test samples. As additional evidence, studies investigating thermal conductivities of pure thermoplastic filaments did not experience a reduction in conductivity at high infill densities [19]. This difference in behavior is presumably attributed to the presence of the chopped carbon fibers in the composite Onyx filament. In transverse samples a greater drop in thermal conductivity was observed than longitudinal samples when interconnecting infill layers occur likely because of the fibers being perpendicular from the direction of heat flow, emphasizing this effect to a greater extreme. Additionally, these reductions at high infill density may also be attributed to trapped air pockets.

In conclusion of this study, to maximize the thermal conductivity of chopped fiber composite prints a high infill density should be implemented with the print layup and fiber orientation in the direction of heat flow. To achieve the lowest effective thermal conductivity the least amount of infill density should be used along with orientation of fibers perpendicular to the direction of heat flow.

8.4 Study and Setup Improvements

While improved from the previous system, several revisions can still be made to the experimental setup to increase measurement capabilities. First, a new chiller should be obtained for any future studies. The current chiller was unable to cool past ambient room temperature. A sufficient temperature gradient and heat flow were still achieved for testing. However, the cycle time per test suffered as it took longer to reach a steady temperature for data collection. As an extra precaution, temperature values were taken from a steady state period twice as long as the recommended ASTM D5470 steady state time to ensure accuracy. The long experimentation

time hindered the number of trials able to be completed in the timeframe of this study. A new recirculating chiller will improve testing efficiency and potentially data quality.

As seen in Fig 20, the root cause of the mistrial data is inconsistent contact resistance between samples within a data set, distorting calculations. While improvements were made to grease deposition and loading methods, better systems to ensure consistent load application need to be implemented. More testing of isotropic materials with known thermal conductivities should be conducted to help better gauge system accuracy and improve the correction factor. Thermistors could be implemented to improve meter bar temperature readings. Thermistors provide higher accuracy and less noise than thermocouples. They could be spaced with smaller increments and in closer proximity to the sample surface, improving the surface temperature and heat flow estimations and therefore increasing accuracy of the system.

Additionally, it is recommended to have meter bars of the same lengths. However, due to material constraints, a smaller cold meter bar was used with closer spaced thermocouples. Symmetrical meter bars may yield some improvement to system accuracy. For the hot meter bar, the cartridge resistance heaters can be integrated into the top face, eliminating the need for the hot plate and removing one thermal interface.

8.5 Future Work

In continuation of this study more infill patterns should be evaluated aside from the standard rectangular infill geometry, such as triangular and gyroid, to determine if for other infill patterns increasing density will result in an increase in thermal conductivity. To further evaluate the impact of fiber angles on thermal conductivity, more longitudinal samples should be produced with varying infill angles to create infill layups in the direction of heat flow at varying fiber angles. From these trials a relationship relating fiber angle to thermal conductivity can be

developed. A longitudinal sample with infill deposits laid parallel to the direction of heat flow should be made to determine if these experimental trends and the phenomena of reducing thermal conductivity at very high infill densities are consistent with fiber angle. If this sample at 100% infill yields the highest thermal conductivity, then the reduction due to fiber angle offset to system heat flow is confirmed.

Samples may also be tested on other setups as confirmation trials. Testing samples of several types of chopped fiber composites can be performed to determine if the observed phenomena are consistent between chopped fiber FDM printed materials. The thermal conductivity of the carbon fiber laminate in the longitudinal direction should also be evaluated to compare to the longitudinal thermal conductivity of the Onyx printed samples. Additionally, more simulations can be performed comparing the thermal conductivity of laminate materials to that of isotropic materials in longitudinal and transverse directions.

A higher conductivity composite filament, such as copper particles mixed with a thermoplastic matrix, could be used to achieve a more discernable difference between sample values with higher resolution in data. This would better quantify the relationships between infill density and patterns on thermal conductivity.

To truly evaluate the impact the direction of heat flow has on effective thermal conductivity based on infill pattern orientation, this study should be repeated with samples of a pure thermoplastic. Pure thermoplastic filaments that do not have fiber reinforcement will eliminate the influence of fiber orientation on effective thermal conductivity. This will allow differences in thermal conductivity to be attributed mainly to the geometry of the sample rather than another heavily influencing factor.

A second set of samples with varying print processing parameters aside from infill density could also be produced. Variations of the printing parameters specified in section 2.3 can be performed to determine their influence on sample thermal conductivity. Additionally, more samples per data set should be printed and tested to ensure that differences in data are not due to process influences or defects beyond the tested infill density and orientation criteria.

Chapter 9: Appendix

Table 11. Overview of experimental data.

Sample Category	Infill Percentage	Infill Pattern	Layup Direction	Conductivity K Removing Cont. R. (W/mK)	Thermal Interfacial Resistance (Ri)	*Sample Height (m)	*Temperature Hot (C)	*Dt/Dh Hot	HMB Q (W)	*Temperature Cold (C)	*Dt/Dh Cold	CMB Q (W)	Avg. Heat Flow Q (W)	Thermal Impedence (k*m^2)/W
Acrylic no grease	-	-	-	**1.7513**	0.0030	0.0015	*51.3970*	*20.7828*	16.4504	*27.5672*	*10.9621*	8.6770	12.5637	0.0038
						0.0030	*57.8110*	*20.9678*	16.5969	*27.5603*	*11.9831*	9.4851	13.0410	0.0047
Acrylic	-	-	-	**1.0138**	0.0020	0.0015	*48.8924*	*18.6027*	14.7248	*28.2402*	*11.4615*	9.0723	11.8985	0.0035
						0.0030	*54.1063*	*18.0844*	14.3146	*27.2814*	*9.3968*	7.4379	10.8763	0.0050
303 Steel	-	-	-	**20.7164**	0.0001	0.0055	*30.4312*	*20.9023*	16.5450	*28.4137*	*11.9329*	9.4454	12.9952	0.0003
						0.0099	*31.7051*	*20.2183*	16.0036	*28.3624*	*12.2499*	9.6963	12.8499	0.0005
Retrial CF Sheet	-	**0/90 Laminate**	**Transverse**	**1.3288**	0.0032	0.0032	*43.1716*	*3.5543*	2.8134	*24.6110*	*13.5575*	10.7313	6.7723	0.0055
						0.0063	*51.2213*	*3.4526*	2.7329	*25.1527*	*13.3557*	10.5716	6.6523	0.0079
Extruded CF Sheet	-	**0/90 Laminate**	**Transverse**	**1.3065**	0.0017	0.0032	*44.4931*	*11.7833*	9.3270	*26.5201*	*10.6786*	8.4525	8.8898	0.0041
						0.0063	*51.5464*	*11.8973*	9.4172	*24.1166*	*9.6270*	7.6202	8.5187	0.0065
ONYX 100%	**100%**	**Solid/Rectilinear**	**Transverse**	**2.4464**	0.0025	0.0100	*62.5197*	*20.6600*	16.3532	*26.6125*	*7.3300*	5.8020	11.0776	0.0066
						0.0050	*58.7389*	*23.7317*	18.7846	*28.3766*	*10.6377*	8.4202	13.6024	0.0045
ONYX 100%	**100%**	**Solid/Rectilinear**	**Longitudinal**	**3.2375**	0.0023	0.0100	*60.4238*	*21.2360*	16.8091	*28.5219*	*9.0592*	7.1707	11.9899	0.0054
						0.0050	*51.2221*	*21.4249*	16.9587	*26.1272*	*11.9815*	9.4839	13.2213	0.0038
ONYX 100%	**100%**	**Solid/Rectilinear**	**Longitudinal**	**3.8920**	0.0030	0.0100	*60.8729*	*22.1550*	17.5366	*25.4946*	*10.1861*	8.0627	12.7996	0.0056
						0.0050	*53.6184*	*20.8668*	16.5169	*26.3483*	*11.4887*	9.0938	12.8054	0.0043
ONYX 92%	**92%**	**Rectangular**	**Transverse**	**3.0340**	0.0030	0.0100	*61.8511*	*20.4196*	16.1629	*23.7913*	*10.6932*	8.4641	12.3135	0.0063
						0.0050	*52.8913*	*22.2495*	17.6114	*22.8756*	*11.0572*	8.7522	13.1818	0.0046
Onyx 77%	**77%**	**Rectangular**	**Transverse**	**4.2434**	0.0025	0.0100	*61.3485*	*29.9375*	23.6967	*26.1654*	*7.0907*	5.6126	14.6547	0.0049
						0.0150	*65.8216*	*24.3705*	19.2902	*28.2292*	*7.4750*	5.9168	12.6035	0.0060
ONYX 55%	**55%**	**Rectangular**	**Transverse**	**3.4740**	0.0027	0.0100	*64.3111*	*27.3254*	21.6292	*25.6082*	*8.1840*	6.4780	14.0536	0.0056
						0.0050	*59.4332*	*32.4739*	25.7044	*26.0866*	*8.7638*	6.9369	16.3207	0.0041
ONYX 33%	**33%**	**Rectangular**	**Transverse**	**1.5970**	0.0017	0.0100	*65.9425*	*17.8793*	14.1522	*25.8541*	*7.9454*	6.2891	10.2206	0.0079
						0.0050	*58.9915*	*26.8194*	21.2287	*25.8196*	*8.4544*	6.6920	13.9603	0.0048
ONYX 33%	**33%**	**Rectangular**	**Transverse**	**2.4882**	0.0028	0.0100	*70.5578*	*24.8221*	19.6477	*26.0397*	*8.5710*	6.7843	13.2160	0.0068
						0.0050	*58.9915*	*26.8194*	21.2287	*25.8196*	*8.4544*	6.6920	13.9603	0.0048
ONYX 10%	**10%**	**Rectangular**	**Transverse**	**1.5759**	0.0020	0.0100	*64.3345*	*15.4400*	12.2214	*24.2875*	*9.0433*	7.1582	9.6898	0.0084
						0.0050	*62.0948*	*28.2823*	22.3866	*24.1228*	*9.1073*	7.2088	14.7977	0.0052
ONYX 92%	**92%**	**Rectangular**	**Longitudinal**	**4.3720**	0.0033	0.0100	*57.4632*	*21.2276*	16.8025	*24.3945*	*9.1773*	7.2642	12.0333	0.0056
						0.0050	*56.1781*	*23.3176*	18.4568	*28.9862*	*8.1510*	6.4519	12.4543	0.0044
ONYX 77%	**77%**	**Rectangular**	**Longitudinal**	**3.6088**	0.0027	0.0100	*63.2632*	*19.2437*	15.2322	*27.7972*	*13.9446*	11.0378	13.1350	0.0055
						0.0050	*56.4951*	*27.0369*	21.4008	*28.4518*	*8.1120*	6.4210	13.9109	0.0041
ONYX 55%	**55%**	**Rectangular**	**Longitudinal**	**3.1621**	0.0024	0.0100	*63.1190*	*25.0591*	19.8353	*26.3611*	*8.6902*	6.8786	13.3570	0.0056
						0.0050	*58.2375*	*29.7647*	23.5600	*27.6521*	*9.4420*	7.4737	15.5168	0.0040
ONYX 33%	**33%**	**Rectangular**	**Longitudinal**	**3.1455**	0.0025	0.0100	*65.5270*	*27.4034*	21.6909	*28.0860*	*6.4035*	5.0686	13.3798	0.0057
						0.0150	*66.8519*	*20.0725*	15.8882	*26.1706*	*8.6133*	6.8178	11.3530	0.0073
ONYX 10%	**10%**	**Rectlinear**	**Longitudinal**	**2.5632**	0.0041	0.0100	*66.9128*	*20.9550*	16.5867	*24.3403*	*6.3492*	5.0257	10.8062	0.0080
						0.0050	*57.8311*	*17.6652*	13.9828	*22.3058*	*12.4933*	9.8890	11.9359	0.0060

Table 12. COMSOL Simulation data and results.

Sample Category	Layup Direction	*Sample Height (m)	**Simulated Conductivity (W/mK)**	*Temperature Hot (C)	*Temperature Cold (C)	DT/DH	Avg. Heat Flow Q (W)	Thermal Impedence (k*m^2)/W
33%	**Transverse**	0.010	4.1933	*427.7223*	*393.1491*	*36.2443*	1.4498	0.0024
55%	**Transverse**	0.010	4.6805	*420.1951*	*392.0046*	*32.9867*	1.3195	0.0021
77%	**Transverse**	0.010	4.7114	*414.6805*	*390.7276*	*28.2127*	1.1285	0.0021
33%	**Long**	0.010	1.4418	*443.4590*	*392.3866*	*18.4086*	0.7363	0.0069
55%	**Long**	0.010	2.1348	*429.5684*	*391.4974*	*20.3184*	0.8127	0.0047
77%	**Long**	0.010	2.8930	*419.8934*	*390.4341*	*21.3065*	0.8523	0.0035

Chapter 10: Bibliography

1. Onyx - composite 3D printing material. November 10, 2025. https://shop.markforged.com/shop/s/product/detail/01t1600000HG2aOAAT

2. Yun, J. H., Yoon, G. W., Jeon, Y. J., & Kang, M. S. Evaluation of the Properties of 3D-Printed Onyx-Fiberglass Composites. *Materials (Basel, Switzerland)*, 2024. *17*(16), 4140. https://doi.org/10.3390/ma17164140

3. Markforged Onyx Filament FFF - 800 Cm3 Spool. Mark3D UK - Markforged partner for 3D printers in the UK, August 15, 2025. https://www.mark3d.com/en/product/filaments-for-markforged-3d-printers/markforged-onyx-filament-fff-800-cm%C2%B3-roll/#.

4. Shanmugam, Vigneshwaran et al. The thermal properties of FDM printed polymeric materials: A review. *Polymer Degradation and Stability*, 2024. 228. 110902. 10.1016/j.polymdegradstab.2024.110902.

5. T. Ludergnani et al., Infill Density Effects on the Mechanical and Thermal Properties of Copper-Plated 3D Printed Parts. *Macromol. Mater. Eng,* 2023. 308, 2300203. https://doi.org/10.1002/mame.202300203

6. Inan, EE, & Saigal, A. "Elastic and Thermal Properties of Additively Manufactured Continuous Fiber Composites." *Proceedings of the ASME 2024 International Mechanical Engineering Congress and Exposition*. Portland, Oregon, USA. November 17–21, 2024. V003T04A015. ASME. https://doi.org/10.1115/IMECE2024-144132

7. Thermal Conductivity Methods: Transient vs Steady-State. Selecting the Right Method: Transient vs Steady-State for Thermal Conductivity Measurement. Accessed January 8, 2026. https://thermtest.com/transient-vs-steady-state-for-thermal-conductivity-measurement.

8. Bulinski et al. Application of the ASTM D5470 standard test method for thermal conductivity measurements of high thermal conductive materials. *Journal of Achievements in Materials and Manufacturing Engineering*, 2019. 2. 57-63. 10.5604/01.3001.0013.7915.

9. ASTM D5470-12 Standard Test Method for Thermal Transmission Properties of Thermally Conductive Electrical Insulation Materials, 2017

10. Aboras et al. Limitations and Accuracy of Steady State Technique for Thermal Characterization of Thermal Interface Materials and Substrates, 2014. 10.1109/ITHERM.2014.6892429.

11. Kempers et al. A high-precision apparatus for the characterization of thermal interface materials. *The Review of scientific instruments*, 2009. 80. 095111. 10.1063/1.3193715.

12. Multipurpose 110 Copper Sheets and Bars. McMaster. Accessed January 17, 2026. https://www.mcmaster.com/products/copper-alloy-110/copper-2~/multipurpose-110-copper-sheets-and-bars-8/?s=copper-alloy-110.

13. Marc Hodes, Professor of Mechanical Engineering, Tufts University - Private Communication, 2025

14. Elkholy et al. An accurate steady-state approach for characterizing the thermal conductivity of Additively manufactured polymer composites. *Case Studies in Thermal Engineering* 31, 2022. 101829. 10.1016/j.csite.2022.101829.

15. AISI Type 303 Stainless Steel, Cold Drawn Bar, Tested at RT. ASM material data sheet. Accessed January 7, 2026. https://asm.matweb.com/search/specificmaterial.asp?bassnum=mq303h.

16. Overview of materials for acrylic, extruded. Accessed January 7, 2026. https://www.matweb.com/search/datasheet_print.aspx?matguid=632572aeef2a4224b5ac8fbd4f1b6f77.

17. Joven, Ronald et al. Thermal properties of carbon fiber/epoxy composites with different fabric weaves, *SAMPE International Symposium Proceedings At: Charleston, SC*, 2012.

18. Overview of materials for PA6 (nylon 6), extruded. Accessed January 7, 2026. https://www.matweb.com/search/DataSheet.aspx?MatGUID=726845c457b94b7cafe31d2e65739e1d.

19. Tychanicz-Kwiecień, Maria & Grosicki, Sebastian & Markowicz, Marek. Experimental Investigation of Thermal Conductivity of Selected 3D-Printed Materials. *Materials,* 2025. 18. 3950. 10.3390/ma18173950.

20. Bao Y, Ma Y, Yang Y, Wang J, Cheng D. Study on the effect of carbon fiber ply angle on thermal response of CFRP laminate based on the thermal resistance network model. *Polym Compos*. 2023; 44(12): 8792-8804. doi:10.1002/pc.27737

21. Michael Zimmerman, Professor of Mechanical Engineering, Tufts University ME116 – Composite Materials, Class Lecture Notes, 2025

22. Audrey - McMaster Carr Support, Private Communication. High-Strength Lightweight Carbon Fiber Sheet 8181K16. McMaster. 2025.

23. Bard, S., Schönl, F., Demleitner, M., & Altstädt, V. Influence of Fiber Volume Content on Thermal Conductivity in Transverse and Fiber Direction of Carbon Fiber-Reinforced Epoxy Laminates. *Materials*, 2019. *12*(7), 1084. https://doi.org/10.3390/ma12071084

24. Gu-Hyeok Kang, Myungsoo Kim, Young-Bin Park, Enhanced thermal properties of tensile-aligned chopped carbon Fiber/HDPE composites for one-directional thermal ventilation, *Polymer Testing*, Volume 135, 2024, 108445, ISSN 0142-9418,

25. Compton BG, Lewis JA. 3D-printing of lightweight cellular composites. *Adv Mater*. 2014 Sep 10;26(34):5930-5. doi: 10.1002/adma.201401804. Epub 2014 Jun 18. PMID: 24942232.

26. Prasanthi, P.P., Ramacharyulu, D.A., Babu, K.S. et al. Role of fiber orientation and design on thermal and mechanical properties of natural composite. *Int J Interact Des Manuf* 19, 2025. 1383–1393. https://doi.org/10.1007/s12008-024-02042-3